

Charting Brain Development in Graphs, Diagrams, and Figures from Childhood, Adolescence, to Early Adulthood: Neuroimaging Implications for Neuropsychology

Erin D. Bigler^{1,2,3,4,5} 

Received: 14 February 2021 / Revised: 14 February 2021 / Accepted: 15 March 2021 / Published online: 25 May 2021
© American Academy of Pediatric Neuropsychology 2021

Abstract

The role of magnetic resonance (MR) neuroimaging in studying brain development in the first three decades of life is reviewed, in terms of its relevance to pediatric neuropsychology. This review places an emphasis on displaying development neuroimaging findings in various types of growth plots, diagrams and figures. MR imaging (MRI) methods can be divided into both structural and functional approaches for brain development quantification. Since MRI methods can readily separate brain parenchyma into white matter (WM), gray matter (GM), and cerebrospinal fluid (CSF) spaces, depending on the anatomical region or region of interest (ROI), MRI quantification is typically in the form of volume, surface area, shape, and/or thickness. Diffusion tensor imaging (DTI) permits the computation of various quantitative metrics, especially sensitive to WM integrity, including the extraction and assessment of WM tracts. Functional MRI (fMRI) techniques provide physiological metrics that examine maturation through connectivity profiles. Regardless of the MRI method used for image quantification, dynamic changes of the brain occur throughout the first three decades of life, dominated by GM reductions associated with cellular pruning and WM increases, reflecting myelination and connectivity. From a neuroimaging perspective, when quantitative metrics show stabilization, this may be an indication of a neuroimaging-derived “brain age” metric. Future directions and the importance of understanding brain development and neuroimaging findings in the context of neural networks and their maturation as applied to pediatric neuropsychology are discussed.

Keywords Brain development · Quantitative neuroimaging · Brain connectivity · MRI · fMRI · Diffusion tensor imaging (DTI) · Growth plots · Neural networks

This article is part of the Special Issue: Law, Neuroscience, and Death as a Penalty for the Late Adolescent Class; Dr. Robert Larkin, Guest Editor.

✉ Erin D. Bigler

¹ Department of Psychology and Neuroscience Center, Brigham Young University, Provo, UT 84602, USA

² Department of Neurology, University of Utah, Salt Lake City, UT 84132, USA

³ Department of Psychiatry, University of Utah, Salt Lake City, UT 84132, USA

⁴ Department of Neurology, University of California, Davis, Sacramento, CA 95616, USA

⁵ Somerset, USA

The review that follows will be a bit different from traditional reviews of the developing brain in neuropsychology—it will be mostly pictorial. A substantial repository of neuroimaging-based studies¹ focused on brain development now exists. Typically, neuroimaging findings about brain development are summarized in some graphic form as a standard X-Y plot, where the abscissa reflects age and the ordinate displays some type of neuroimaging metric, usually a specific neuroanatomical region or quantitatively derived region of interest (ROI) measure. As such, a rich resource of graphic and figural information about brain development and maturation has been generated. Accordingly, in graphic form, this review brings some of this information together that shows quantitative

¹ This review assumes familiarity with neuroimaging methods and basic image analysis procedures. For additional background on the neuroimaging methods discussed in this review, the reader is referred to the following: Wilde et al., (2012b)

neuroimaging indices of brain development and maturation, with particular relevance for pediatric neuropsychology.

Computed tomography (CT), introduced in the early 1970s (Ambrose & Hounsfield, 1973), was the first non-invasive neuroimaging method for *in vivo* brain imaging. However, CT imaging exposes the individual to radiation, albeit small amounts, and therefore, it is not a compatible method for longitudinal neuroimaging of the brain, especially in healthy infants and children. This all changed with the advent of magnetic resonance (MR) technologies and the introduction of MR imaging (MRI) of the brain in the 1980s, as MRI has no such risks (Ball, 1991). Developmental studies take time, and consequently, it is not until the end of the twentieth century and the beginning of the twenty-first century that well-designed MRI-based neuroimaging investigations focused on brain development in healthy, age-typical individuals were first published (see Courchesne et al., 2000; Pfefferbaum et al., 1994).

Viewing growth plots from neuroimaging investigations is intuitive, as shown in Fig. 1. In one of the first large-scale developmental, yet cross-sectional neuroimaging studies, Courchesne et al. (2000) addressed the relationship between head size, derived from MRI measured as total intracranial volume (TICV), and age as depicted in Fig. 1. Without much discussion or even statistical analysis, these plots show exponential head growth in the first few years of life, which, in turn, stabilizes in mid-to-late childhood, plateauing thereafter. These types of plots allow the immediate visualization of when and where dynamic changes occur over different developmental stages, when they plateau or change in trajectory. Indeed, this is the basis for the growth chart in every pediatrician's office to monitor height, weight, and head circumference (HC). Accordingly, what was shown by Courchesne et al. (2000) and displayed in Fig. 1 was not new, because these MRI-derived TICV plots perfectly mirrored what was already known about head size development by plotting HC by age (Serru et al., 2019). However, what Courchesne et al. (2000) demonstrated was that the MR image could be

quantified, indicating ground-truth replication of what occurred with direct, physical measurement of HC.

Prior to contemporary neuroimaging, HC was the only physical measurement to infer brain development. Indeed, post-mortem measurements of skull size or intracranial volume accurately estimate brain size (Maxeiner & Behnke, 2008; Yamada et al., 1999). HC as a proxy measure of brain development dates back to the beginnings of pediatrics as a medical discipline (Meredith, 1946). While a proportionally small head represents a biological necessity for the head to exit the birth canal, head size therefore needs to be small at birth. To meet this requirement of smallness, as shown in Fig. 1, head size is ~30% of its ultimate adult size at birth. However, TICV as a reflection of head size rapidly changes as shown in Fig. 1, such that by 1 year, it reaches 70–80% of adult size. While TICV mirrors skull enlargement, the rapid expansion of TICV occurs as a secondary process stimulated by brain growth that drives the increases from total brain volume (TBV). As shown in Fig. 2, the overall positive correlation between HC and TBV exceeds .90 (Serru et al., 2019). For developmental psychology and neuropsychology in monitoring early brain development, the HC measurement offers some clinical utility to infer brain growth, especially for high-risk infants in the first few years of life, like those associated with prematurity, but as HC quickly levels off, it no longer provides a useful metric for neuropsychology. Contemporary neuroimaging methods do because the brain, not just the skull or size of the head can be imaged, as will be further explained throughout this review.

This review will not be hypothesis driven or will not even attempt to test a hypothesis but will merely present, in graphic form, how neuroimaging can be used to display the dynamic changes captured with brain imaging metrics over the first three decades of life. However, there is the assumption that neuroimaging demonstrated brain development and maturation will, in some fashion, parallel behavioral, emotional, and cognitive development, which, in many respects, will display similar growth plots. All psychological, educational, and neuropsychological assessment measures plot some measure of emotional/cognitive/motor/sensory-perceptual and/or educational ability with age, as do neuroimaging studies. Accordingly, throughout this review, these types of growth plots and their intuitive visualization will be the basis for the figures presented, with the assumption that highly interrelated, reciprocal relations between brain and behavior share common roots, paralleling one another, producing similar growth plots.

While there is a substantial literature, both clinical and bench science, on *in utero* and the first 3 years of brain development (Gilmore et al., 2018), this review will only peripherally tap that timeframe. There is a host of neurodevelopmental, genetic, pregnancy, gestational, birth, and related factors associated with *in utero* brain development that will not be part

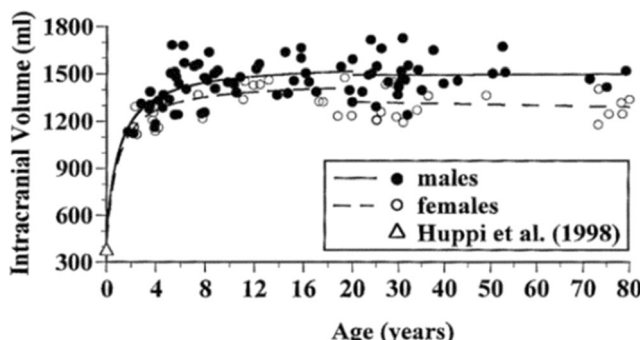
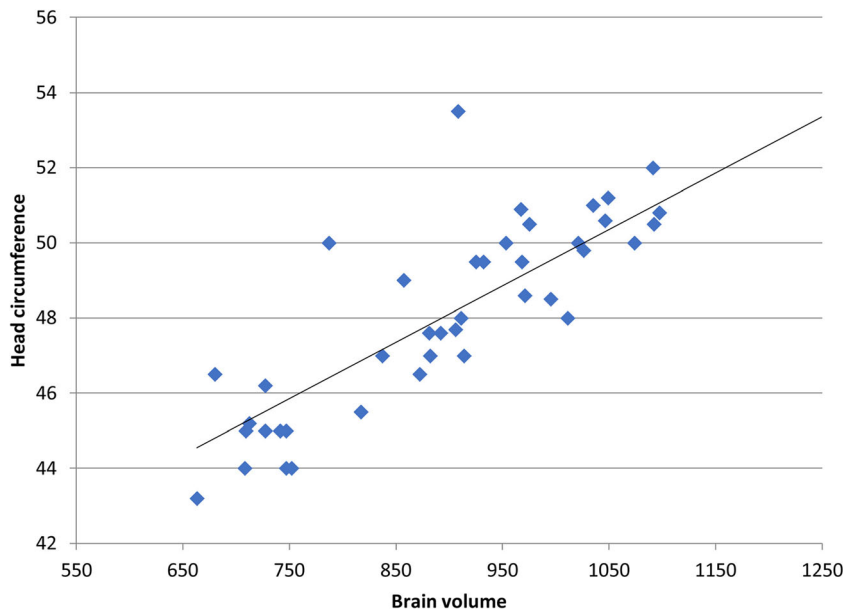


Fig. 1 Total intracranial volume (TICV) by age. Note the rapid increase in TICV over the first few years of life, with general plateauing by late-childhood, mid-adolescence. From Courchesne et al. (2000), used with permission from the Radiological Society of North America

Fig. 2 Correlation between automatically estimated brain volume (ml) and head circumference (cm). From Serru et al. (2019), with permission from Elsevier

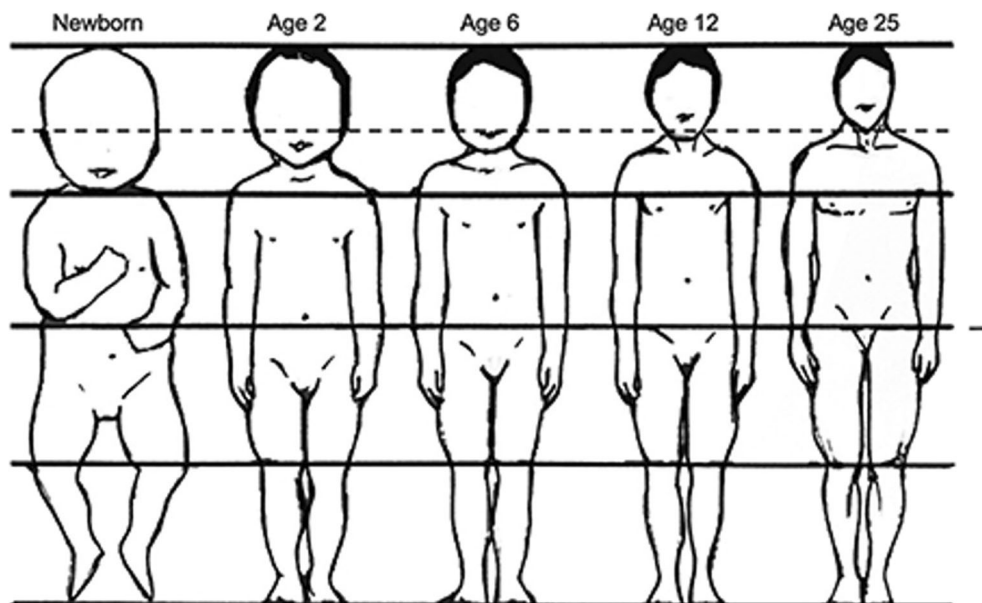


of this review. From a neuropsychological perspective, assessments performed from birth to age 3 are truly just developmental measures. However, starting at age 3, the beginning of what becomes a more standard neuropsychological examination becomes possible (Baron, 2018; Reynolds & Fletcher-Janzen, 2009). Accordingly, this review will typically have age 3 as a lower boundary and will, in turn, concentrate on neuroimaging-derived brain development from this early childhood timeframe through the mid-20 years of life, in other words, the beginning of what is referenced as adulthood.

However, exactly when “adulthood” is attained is debatable. The outward signs of physical development in relation to the head and brain, as illustrated in Fig. 3, are obvious. In fact, it has been evolutionarily assumed that humans acquire innate

visual perceptual abilities to estimate age of another person, merely by looking at that size of an individual, including the proportional differences between head size, physical height, and body morphology (Coma et al., 2014; Murphy, 2011). This perception of outward body size and appearance is part of the social brain network and its development (Freiwald, 2020; Schurz et al., 2020) and has also attracted machine learning, with digital face recognition approaches for estimating age purely from face recognition (Fu et al., 2010). Outward appearance as a sign of maturation, as shown in Fig. 3, depicts the disproportionate size of the head to the body as a reflection of age, where head size actually stabilizes relatively early. But, outward head size could not, alone be an anthropomorphic indicator of adulthood.

Fig. 3 Anthropometric differences between children and adults. The image on the left demonstrates the decreasing head-to-body size ratio from birth to adulthood, adapted from Lindsey et al. (2019) and Pinto et al. (2012)



What metric should be used to define adulthood. Different measures include all sorts of developmental indexes, including physical size, as depicted in Fig. 3; legal definitions (right to vote, drive, military service, etc.); psychometric measures that assess acquisition and progression of cognitive skills; and physiological and biological measures (bone density, growth plates, reaction times, motor skill level, etc.), but what about brain maturation and adulthood? When does the developing brain reach adulthood? Can it be inferred or measured with neuroimaging technology? It may be from a neuroimaging perspective that the visualization of an asymptotic plateau that remains stable in the developing individual is the brain's indicator of adulthood. As such, developmental and lifespan changes associated with brain volumetrics have become the basis for calculating "brain age" as an index of maturity (Anatruk et al., 2020).

Pre-dating neuroimaging and methods for the direct visualization of the brain, all types of inferences about "normal" brain growth and development were all post-mortem based on individuals who purportedly had normal development but died from non-neurological reasons. Many of these post-mortem analyses, however, also were performed on developing brains exposed to some pathological condition or had some type of developmental error (Ernhart, 1991; Eskenazi et al., 1988). Some of these studies not only reported on the overall brain weight but also performed histological analyses like cell counts and size, neuronal configuration, and density along with myelin development, but there were no methods to consistently exam ROI size differences, without time-consuming, meticulous dissection and a post-mortem specimen (see Blinkov & Glezer, 1968).

MRI quantification and developmental studies did not occur immediately after the introduction of this technology. In the beginning, MR methods were limited by low magnetic field strength and lengthy acquisition times, again, like CT not compatible with imaging children, but for different reasons. While MRI did not expose the child to any risk, having to lay as still as possible for minutes at a time without movement was and remains a challenge for doing MR-based neuroimaging studies. Movement distortion makes an MR image unquantifiable. Even more problematic in the beginning of modern neuroimaging was the absence of any automated methods for image quantification, and it all had to be done by hand. Hand tracing ROIs was extremely accurate and considered to be the "gold standard" in the beginning of neuroimaging quantification but incredibly time consuming. To hand trace a few ROIs along with the entire surface of the brain and ventricular system for TBV calculation and other key ROIs, doing it reliably between two raters could take 25+ h per case. Fortunately, with the transition from the twentieth to the twenty-first century, there were rapid advances in image acquisition and analysis techniques (see Bigler, 2017). Still, the early seminal contributions by Courchesne et al. (2000)

and Pfefferbaum et al. (1994), as shown in Fig. 4, began the process of plotting cortical as well as whole-brain gray matter (GM) and white matter (WM) volumetrics from birth on, based solely on quantitative measures extracted from the MR scan image of living individuals. These plots, as shown in Fig. 4, were the first quantitative, *in vivo* investigations, in healthy individuals over the lifespan, and all computations were done using operator-controlled methods. Since MRI, unlike CT, provides a clearer and more distinct delineation between WM, GM, and cerebrospinal fluid (CSF) boundaries (see coronal MRI inset in Fig. 4), the unique contributions of these tissue and fluid types could also be quantified. What emerged from these analyses was that while TBV/TICV stabilization occurs early, WM, GM, and CSF volumetrics were far more dynamic and ever changing through the first three decades of life. Overall, GM peaked early in childhood and then dropped off but continued to change even during traditional timeframes of adolescence and early adulthood. In contrast, WM volume accelerated through early childhood, continuing to increase in volume without plateauing until individuals were in their mid-20s to 30s. MRI-derived CSF volumetrics (not shown) were more stable, once mid-childhood was reached.

The GM and WM distinction and their dynamic changes are particularly important because they represent different aspects of neuron structure. Axons define the neural circuitry of the brain (Holtmaat & Svoboda, 2009), where the majority are myelinated. This unique biological fact gives rise to its "white" appearance and label. WM neuronal circuitry connects with other neurons via dendrites and synapses that form the GM. These distinctions permit inferences about WM to be used in discussions about brain connectivity and GM inferences about neuronal cell body, metabolism, and synaptic integrity.

Based on the aforementioned post-mortem histologic studies of the child's brain that predated modern neuroimaging, it had become well established that GM cellular pruning processes resulted in reduced GM cortical thickness and, concomitantly, that myelination increased with age (Davison & Dobbing, 1966; Herschkowitz & Rossi, 1971). Now, as demonstrated by the studies of Pfefferbaum et al. (1994) and Courchesne et al. (2000), *in vivo* neuroimaging findings of reduced GM volume during development could be used as proxy for cellular pruning and WM volume increase as a proxy index for myelination. While head size, TICV, and TBV all reach a similar asymptote, within the brain itself, dynamic WM and GM growth patterns were occurring, all measurable via quantitative neuroimaging and viewable.

Myelin has high water content (Oishi et al., 2013; Pujol et al., 2006). Since the basis for MR technology is the precession of hydrogen molecules detected by a radiofrequency (RF) wave, referred to as the RF signal, different MR signal characteristics are especially sensitive to myelin. In fact, because

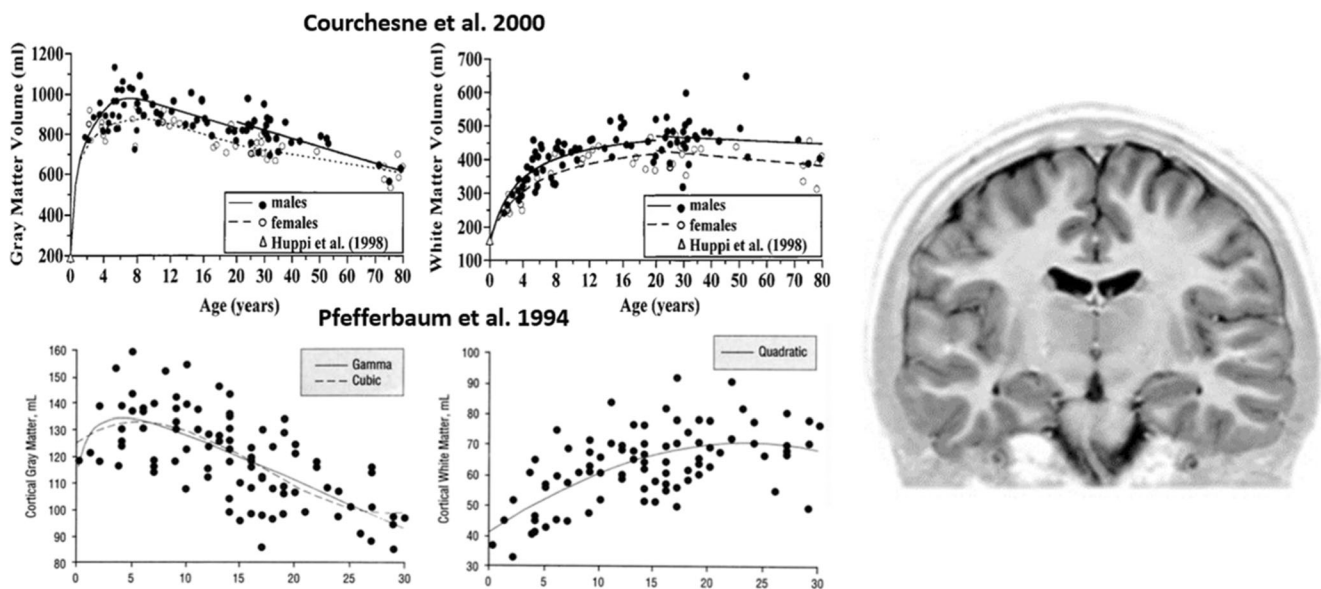


Fig. 4 Developmental changes in gray matter (GM, left) and white matter (WM, right) from Courchesne et al. (2000, top) and Pfefferbaum et al. (1994, bottom). While the investigation of Pfefferbaum et al. (1994) only examined brain development out to 30 years of age, not the robust

similarities between these two completely separate investigations show early peaking of GM development followed by the pruning-mediated decrease, all-the-while prominent increases in WM, reflecting the myelination taking place

of the minimal myelination at birth, there is also minimal differentiation of the MR signal between the WM and GM in the first few months of life (Oishi et al., 2013). Accordingly, by assessing subtle changes in the RF signal starting from birth, when there is minimal WM signal intensity, myelin development can be regionally plotted as it emerges early in life (see Fig. 5). As the WM MR signal changes, depicted as expanding white in Fig. 5, it relates directly to the degree of myelination as well as where myelination is occurring. Pujol et al. (2006) relate these WM changes directly to language and motor skill development, where the growth plots in Fig. 5 are separated by language and sensorimotor areas.

What is visually presented in Fig. 5 is the progression of WM myelination plotted on a sagittal MR image of the infant brain, from a newborn through to a toddler of 3 years of age. Plotting the changes of this MRI-derived myelination coefficient shows how motor and somatosensory regions (see upper panels) of the posterior frontal lobe and anterior parietal respectively come online as the first to show increased myelination after birth, followed by the superior temporal gyrus (lower panels), which houses auditory cortex. These areas of increased myelination map distinctly to the primary motor, somatosensory, and auditory processing networks in the developing brain. What emerge next are the connective WM tracts (arcuate fasciculus) from the auditory cortex in the temporal lobe with motor control centers in the frontal lobe for speech production. Not shown in this particular sagittal plane are the visual cortex and the optic tracts, which also develop rapidly, supporting the visual sensory system as well.

Image Quantification and Neuroimaging-Derived “Brain Age”

As shown in the top left of Fig. 6 (also, see inset in Fig. 4), there are distinct WM, GM, and CSF boundaries in the coronal T1-weighted (W) MRI. If the meninges and skull are stripped away (lower left) and the image converted to conform to a uniform space (also, lower left image), GM, WM, and CSF can be isolated (middle, upper image). Furthermore, because typical neuroanatomy follows a generally similar schematic, using fiduciary and critical landmark identification methods, GM, WM, and CSF regions can be further parcellated and classified (bottom image), using automated algorithms. Isolating the cortical GM mantle (upper right), cortical volume and thickness can be computed as well as gyration and surface area (lower right). The MR image is an average of the different WM, GM, and CSF signal characteristics per the slice thickness of the image. Accordingly, by knowing the slice thickness and number of slices, an assortment of quantitative metrics can be derived from the segmented and classified image.

All of the developmental plots shown up to this point have reflected only global changes in overall brain development. However, with what has now been shown in Fig. 6, based on the segmentation and classification methods of quantitative neuroimaging, the component parts that make up the brain can be quantified as well and their developmental trajectories plotted. Since different regions, cortically or subcortically, have different roles in neural network systems that regulate brain function, these ROIs should also be examined by growth plot analyses and may therefore have different growth patterns

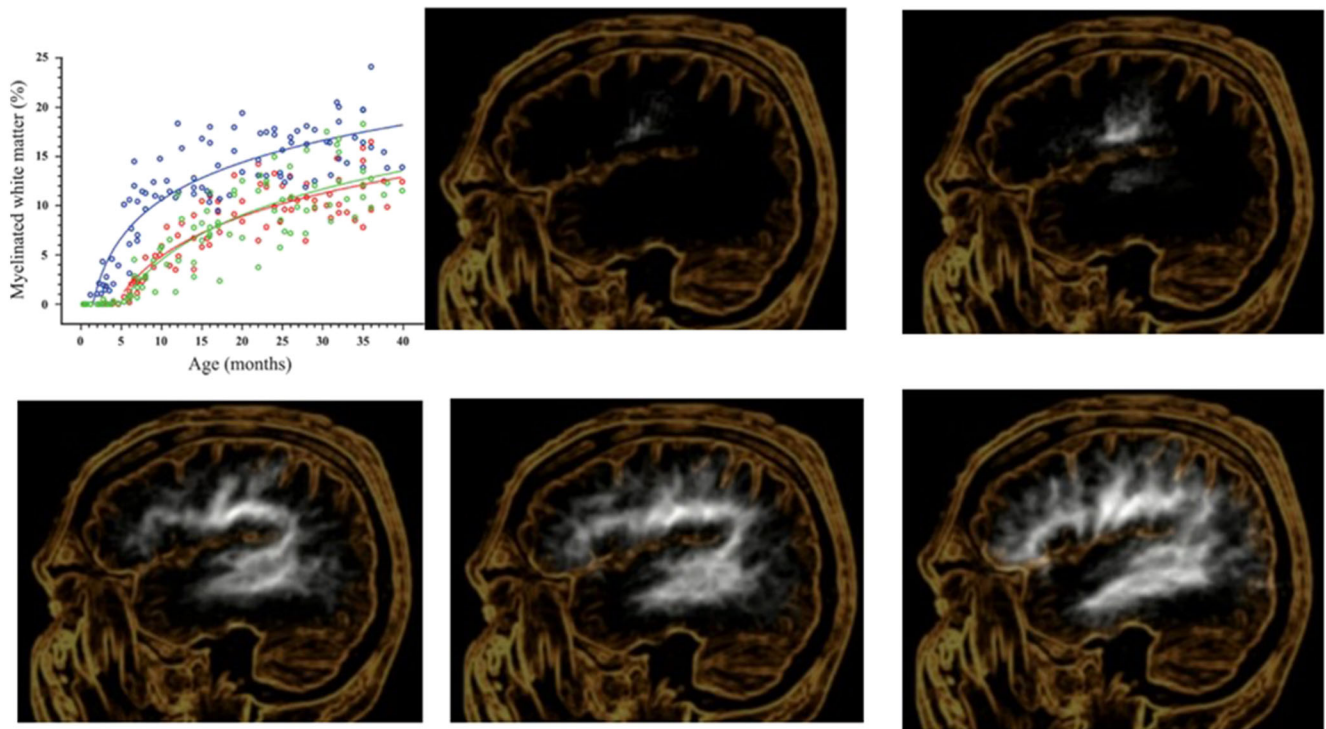


Fig. 5 (Upper left) Plot of age-related increase in relative content of myelinated white matter for the 100 studied children by Pujol et al. (2006). Logarithmic curves for the sensorimotor region (blue), for the temporal region (green) and for the frontal region (red) showing the

volume from myelinated and from non-myelinated white matter (WM). From Pujol et al. (2006), with permission from the American Academy of Neurology and Wolters Kluwer

related to function. Since normal brain development is experience dependent which also relates to neural system development, how can different neuroanatomical regions and neural systems be parsed out and do these cortical and subcortical ROIs further assist in calculating “brain-age” metrics (Franke & Gaser, 2019; Jiang et al., 2019)? With the classified image method shown in Fig. 6, subcortical analyses will be covered toward the end of this section, but first some additional commentary about cortical GM developmental changes.

Figure 7, from Walhovd et al. (2017), shows how cortical thickness and cortical surface area plots relate to brain maturation. While these curves (top image) are similar to what is shown in Fig. 4, this method can also be used to assess the annual rate of change and then plotted on a surface rendering of the brain. Using this approach not only can the whole-brain growth curve be visualized; regional differences can be plotted in what is referred to as a colorized “heat map” (bottom image). Note that the heat map (warm colors) shows the greatest changes in cortical thickness and surface area in the first 10 years of life. Accordingly, as reflected in these growth plots shown in Fig. 7, the dynamic changes that occur in the first decade of life, at the cortical level, slow down thereafter but continue into the 20s.

Vidal-Pineiro et al. (2020) extend the cortical thickness plots out over the entire lifespan, by integrating numerous studies, examined by different age groups, combining them

into the same diagram as shown in Fig. 8. What is important to emphasize in this plot is what would be expected; the most dynamic changes occur within the first three decades of life, followed by a steady decrease in cortical thickness thereafter.

Since it was first shown by Willerman et al. (1991) that intellectual ability positively correlated with TBV, how best to display these types of relations, especially in light of what has been shown so far in terms of cortical GM pruning? At the time of assessment, from a neurobehavioral or neurocognitive perspective, the assumption is that testing assesses the sum total of brain development up to that point of evaluation. As such, neuropsychological variables should also map on to neuroimaging indicators of brain maturation. For example, all intellectual, ability-based and neuropsychological tests make age adjustments. These age corrections assume that increased age reflects age-mediated increased cognitive ability or emotional/behavioral control, which, in turn, reflects maturational brain development. While neurocognitive and neurobehavioral “corrections” for age mirror brain development, to date no standardized neurobehavioral or neurocognitive measure has attempted to integrate a neuroimaging-based brain age coefficient. An example of why this should be the next step in merging brain developmental metrics with neuropsychological assessment and other neurobehavioral measures is the demonstration by Schmitt et al. (2019) in Fig. 9 that shows the dynamic associations between cortical

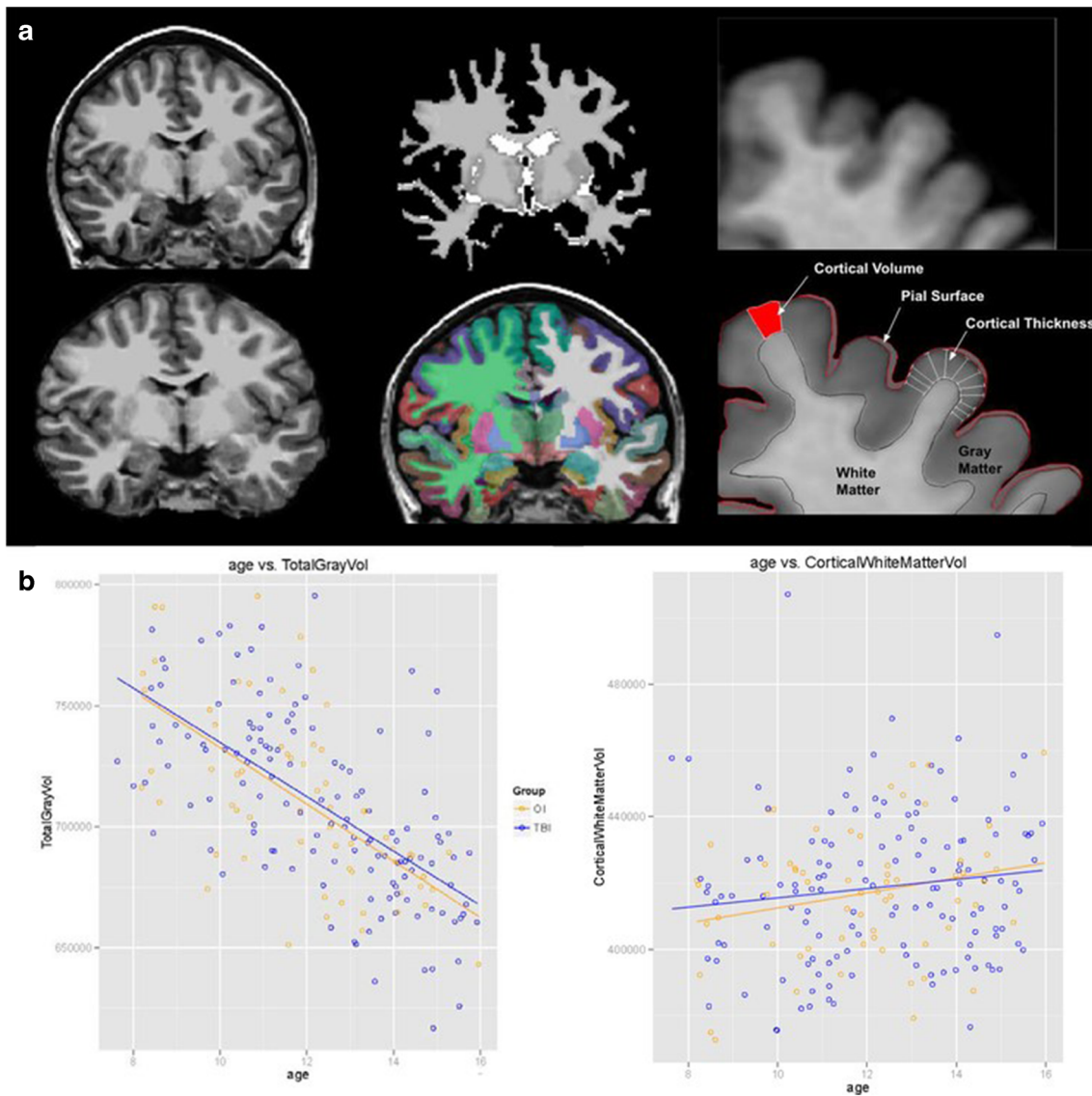


Fig. 6 The picture element, or pixel, intensity in MR imaging reflects tissue type or presence of fluid and/or air in the T1-W sequence shown. Pixel intensity is displayed on a gray scale, where the contrast can be readily determined between the WM and GM as well as CSF-filled spaces as shown on the left, top and bottom coronal images. WM is white, GM is light gray, and CSF is black. Isolating these tissue types, be segmenting them apart, allows the computation of ROI volume for overall WM, GM, and/or CSF volumes, which is shown in the upper middle image. The bottom left image depicts the coronal image with the skull and meninges

removed. This process isolates just the brain, which is then placed within a uniform space. Sophisticated algorithms classify the segmented parenchyma into identifiable anatomical regions or ROIs, referred to as image classification (bottom middle image). Classification schemas following traditional structural identification, such as subcortical ROIs or cortically, cataloging the ROI by Brodmann areas. As illustrated on the right, cortical volume along with the thickness of the cortical ribbon and cortical surface area can be computed

thickness and full-scale intellectual ability from childhood into adolescence. As shown in Fig. 9, widespread changes in cortical thickness and surface area relate to intellectual development as well. Note regional by age differences. Additional commentary about this figure will be discussed in the section on brain networks and the conclusions to this review.

Another takeaway from Fig. 9 applies to the child with an acquired brain injury. Whatever stage of development the brain is in when injury, infection, or some type of acquired pathology strikes will also influence how brain cognitive-

intellectual development and relations proceed thereafter within a neurodevelopmental context toward adulthood, in the now damaged brain (Ewing-Cobbs et al., 2016; Ryan et al., 2020; Wilde et al., 2020). Furthermore, the staging of brain development during childhood and adolescence appears to be critical in terms of any number of neuropsychiatric disorders. As such, understanding brain development in relation to neurocognitive and neurobehavioral development and their intricate relationships with the onset and vulnerability to or emergence of certain neuropsychiatric disorders will likely

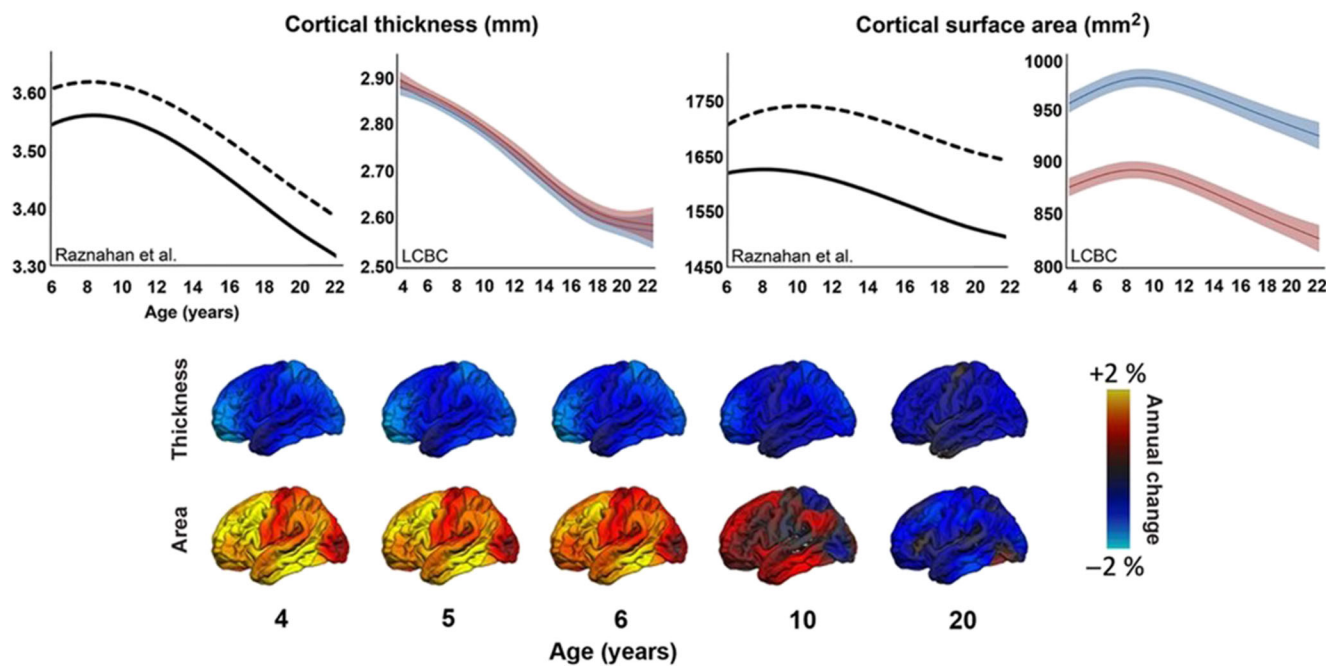


Fig. 7 Developmental trajectories of cortical thickness and area. Upper panel: Comparison of the developmental trajectories reported in Raznahan et al. (2011) to some to data from the Center for Lifespan Changes in Brain and Cognition (LCBC) program, University of Oslo, illustrates some discrepancies across studies. While the surface area shows similar inverse U-shaped trajectories, with larger absolute area for boys (dotted and blue lines) than for girls (solid and red lines), thickness results differ markedly between studies. In Raznahan et al. (2011), thickness increases until approximately 8.5 years, and boys have thicker cortex than girls throughout the age range. In the LCBC data, thickness

shows a monotonic decrease from 4 years, with comparable absolute thickness estimates for boys and girls. Of note, thickness and area are more different in terms of trajectory and sex effects in the LCBC data than in Raznahan et al. (2011). Error bars for the LCBC curves represent 95% confidence interval. Lower panel: Vertex-wise annualized rates of change in cortical thickness and surface area computed in 778 subjects aged 3–20 years from the PING study. As can be seen, cortical thickness decreases monotonically within this age range, while area shows an inverted U-shaped pattern of increase followed by a decrease. From Walhovd et al. (2017), used with permission from Oxford University Press

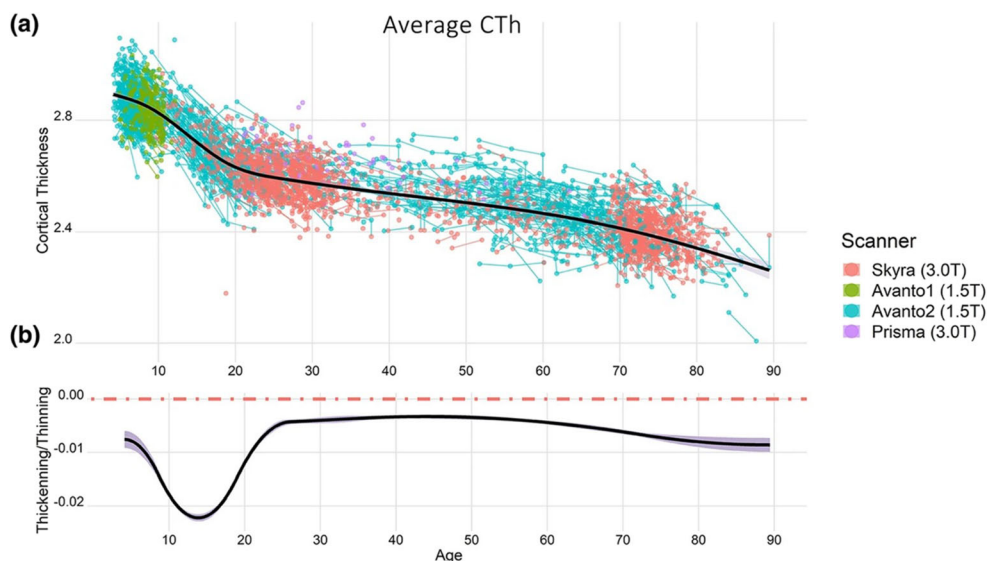
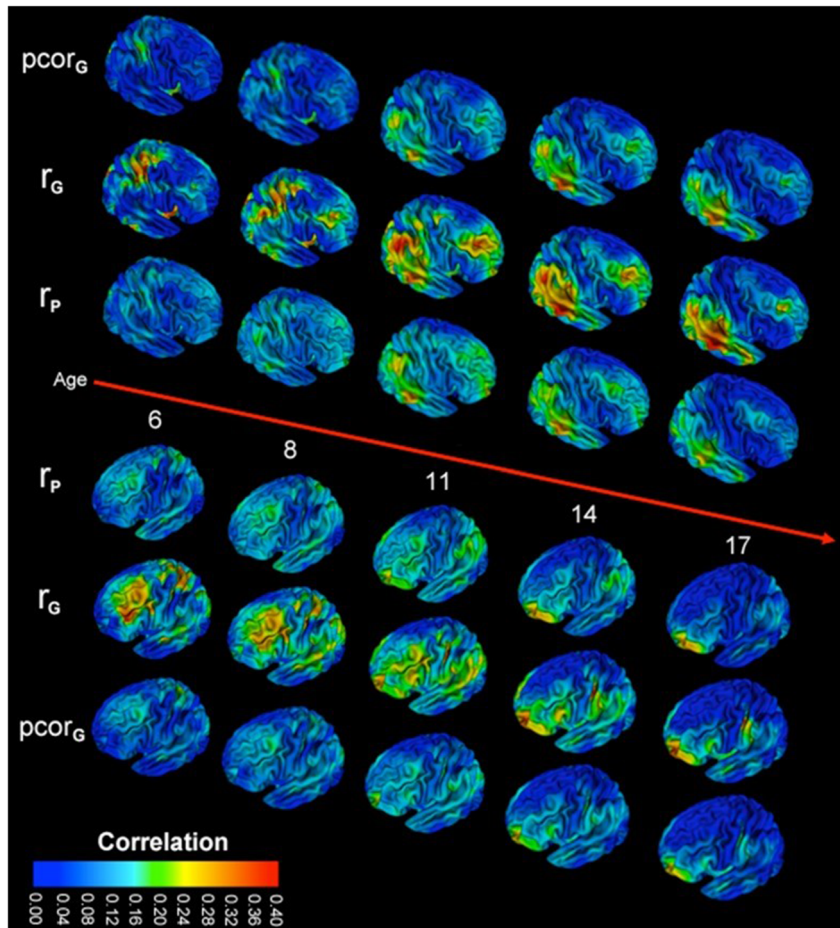


Fig. 8 Trajectories of weighted-average cortical thickness. The upper and lower plots exhibit the trajectories of **a** cortical thickness and **b** cortical thinning during the lifespan, respectively. Cortical thickness fitting (black line) overlies a spaghetti plot that displays each observation (dots), participant (thin lines), and scanner (color). All estimates are adjusted for sex and scanner (scanner platform is displayed on the right). The y-axis units

represent mm and Δmm/year for the thickness and thinning plots, respectively. The dotted red line in the cortical thinning graph represents 0 change, and negative and positive values represent thinning and thickening, respectively. From Vidal-Pineiro et al. (2020), with permission from the Nature Publishing Group

Fig. 9 Dynamic changes between cortical thickness and Full Scale IQ over childhood and adolescence. Maximum likelihood estimates of the phenotypic correlation (r_P), genetic correlations (r_G), and the genetic contribution to covariance ($pcor_G$) shown for ages 6–17. From Schmitt et al. (2019) where changes with time can be viewed dynamically in the Supplementary Movies. Additional views are also provided in Figure S1 at the publication site. Reproduced with permission from Oxford University Press

This document is copyrighted by the American Psychological Association or one of its allied publishers. This article is intended solely for the personal use of the individual user and is not to be disseminated broadly.



yield greater diagnostic specificity and potential therapeutic avenues for treatment, if more can be understood about neuroimaging-derived brain-aging dynamics, behavior, and cognition.

Quantitative Neuroimaging and Microstructure Inference

As already alluded to, MR images approximate the visual appearance of the living brain, or what is referred to as the macro-structure, something akin to interrogating brain parenchyma at autopsy. However, understanding even more about what makes up the image allows both the researcher and clinician the ability to make inferences about the underlying micro-structure of the brain. The illustration from Novikov et al. (2019) presented in Fig. 10 demonstrates the point that at the most elemental level, all aspects of living, viable tissue begin with molecules. How those molecules assemble and organize to create amino acids that form the building blocks for tissue, blood, and CSF, represents the fundamentals of brain development. What is shown at the molecular level can only be assessed with nanometer (nm) precision (a

billionth of a meter; left side of Fig. 10), such as with an electron microscope. In contrast, cell bodies can be viewed with a microscope with micron (μm)-level precision (millionth of a meter; middle image, Fig. 9), but still below what contemporary *in vivo* neuroimaging can achieve. Most commonly, MR-based neuroimaging views tissue at the millimeter (mm) level of resolution, as highlighted in Fig. 10 (right image).

What does mm precision imply for MR metrics assessing GM in studying brain development? It has been estimated that the human brain is comprised of ~80–100 billion neurons (Herculano-Houzel, 2009). Insel and Landis (2013) estimate that within a single, 1-mm³ MRI voxel, it contains "... 80,000 neurons and 4.5 million synapses" (p. 565). Accordingly, at the macroscopic MRI level, even for a small ROI of just a few cubic millimeters, this would reflect hundreds of thousands to millions of neurons. Since glial cells outnumber neurons, what is represented within a single voxel, just from a cellular count, would be even higher (Herculano-Houzel, 2009).

Figure 11, from Veraart et al. (2020), depicts an even better portrayal of this principle, using a rat brain where an MRI scan was obtained in the sagittal plane, with the distinct appearance of an entirely normally appearing corpus callosum, as

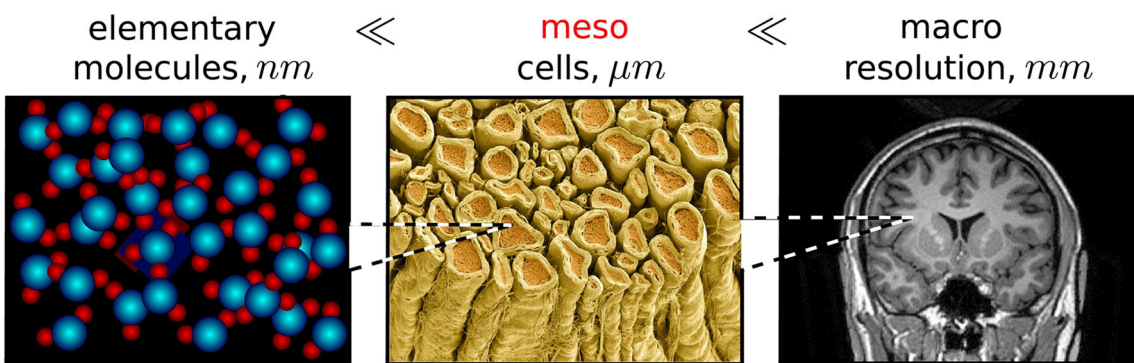
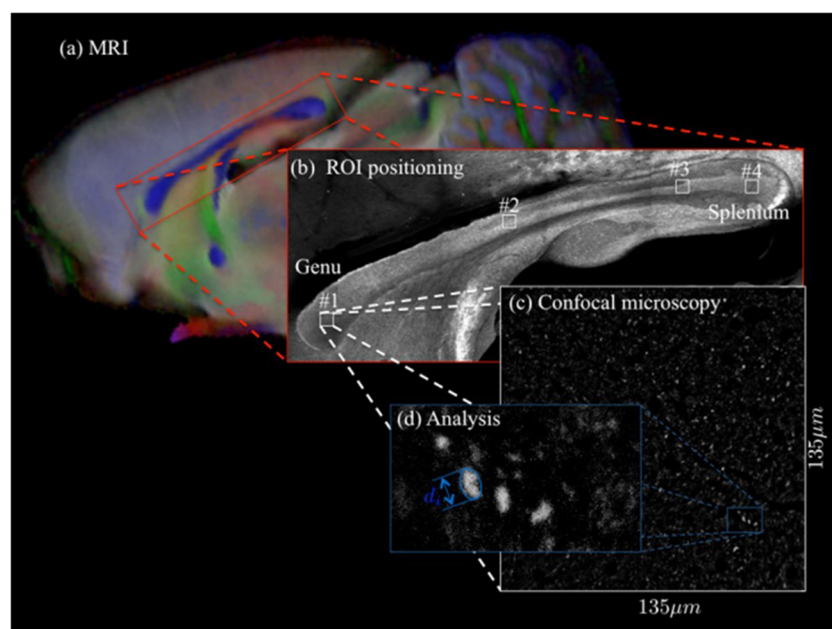


Fig. 10 The mesoscopic scale in brain MRI, as an intermediate scale between the elementary (molecular) and the macroscopic (resolution) from Novikov et al. (2019), reproduced with permission from Wiley

highlighted in the middle image. However, these investigators also examined the brain histologically (lower right). Note, to actually examine the cellular makeup of the corpus callosum, histological analysis at the micron level is required. What this means for neuroimaging and pediatric neuropsychology inferences is that MRI metrics derived from healthy, age-typical individuals form a normative sample, where the average for GM measurements is a proxy for GM integrity that includes cell count, organization, and density, with WM quantifications reflecting myelination, myelin/glial cell count, and compactness of WM tracts (Bigler, 2017). Accordingly, in reference to normative standards for size, volume, thickness, shape, or basic RF signal findings (i.e., water diffusion coefficients), the MR image provides a number of approaches to infer normality or deviation therefrom in the microstructure of brain development. As already implied, this also means that reliable yet subtle differences or changes in MR metrics may signify important neurobiological and neuropathological findings in brain development.

Fig. 11 For two brain samples, MR scanning (a, color encoded FA map) was followed by low (b) and high (c) resolution confocal microscopy with staining for neurofilaments to identify the axons. The low-resolution image was used to position various ROIs, whereas the axon caliber distributions were extracted from the high-resolution image of the corresponding ROIs. The long axes of fitted ellipsoids served as proxies for the respective axon diameters (d). From Veraart et al. (2020) with permission

MR technologies provide multiple methods to query and infer what might be occurring at the microstructure level. Up to this point, the MR image sequences for typical volumetric analyses, and the ones shown so far in this review, have been based on T1-W, T2-W, or some combination of these sequences. The MR sequence label has to do with the timing and duration of when the strong magnetic field used to generate the image is pulsed. T1-W sequences are often referred to as the “anatomical” sequence and, regularly, the basis for many types of quantitative analyses. T2-W sequences provide more distinct visualization of CSF and certain types of intraparenchymal pathologies. Because of its sensitivity to water, combined with the fact that myelin has a high water content, T2-W sequences are particularly useful in the examination of WM. Figure 12, by Silk et al. (2016), displays and compares the image appearance of the most common structural MRI sequences, which all have different sensitivities in detecting diverse aspects of neuroanatomy and neuropathology. Also shown in Fig. 12 is functional MRI (fMRI). In



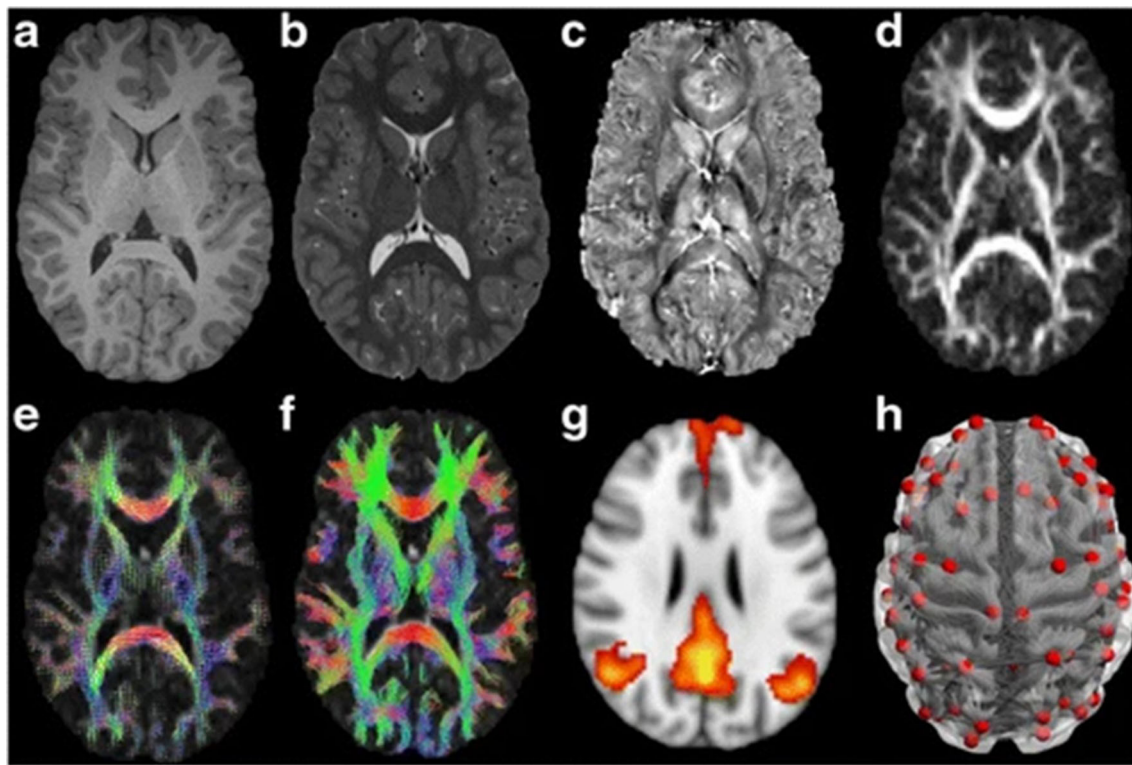


Fig. 12 Examples of the different MR sequences to evaluate structural and functional development. **a** T1-weighted. **b** T2-weighted. **c** Quantitative susceptibility mapping. **d** Diffusion-weighted imaging: fractional anisotropy (FA) map. **e** Diffusion-weighted imaging: estimation of

the fiber orientation distribution. **f** Diffusion-weighted imaging: whole-brain tractography. **g** Resting-state fMRI showing default mode network. **h** Connectivity network for structural and function connectivity from Silk et al. (2016), used with permission

Fig. 12, the T1-W sequence, as already indicated, is often used for general ROI quantification but the principles discussed next in terms of tissue thresholding, segmentation, and classification are similar regardless of which sequence is used. Because of their sensitivity in detecting pathology, T2-weighted MR sequences are often used to isolate abnormalities and compute various quantitative metrics, such as lesion burden. Susceptibility-weighted imaging (SWI) sequences are depicted in Fig. 12c, which readily detect different aspects of the vasculature, as well as hemorrhage, including hemosiderin as a residual by-product from prior hemorrhage. Figure 12d–f represents diffusion tensor imaging (DTI) techniques, which will be further explained in a subsequent section. Figure 12g represents the activation patterns associated with fMRI-based methods for detecting the blood-oxygen-level-dependent (BOLD) MR signal. Because of differences in the magnetic properties of oxygenated versus de-oxygenated blood, those differences echo where the greatest activation has occurred. Versions of this fMRI methodology can also assess cerebral perfusion (van Osch et al., 2018). Finally, all of these methods can be integrated to study brain networks, which will be more fully discussed at the end of this review and/or integrated into what is referred to as a multi-modality quantification of brain metrics to improve detection of differences in normal development as well as disease and injury (see Bigler et al., 2016;

Wilde et al., 2020). However, for this review, the focus will remain mostly on single-modality MR imaging findings related to brain development.

Three-Dimensional Image Quantification and Display

Once image classification can be achieved (see Fig. 6), all aspects of coarse brain structure can be placed into three-dimensional (3-D) space, as shown in Fig. 13, which can be achieved with any image sequence, although what is shown in Fig. 13 is T1-W based. As noted in Fig. 6, gyral patterns can be quantified, as a gyration index, which provides a surface area indicator, readily observable in the upper left image of Fig. 13, which also has each gyrus separately identified. The cortical GM mantle can be removed, exposing the underlying cortical-level WM (top, left middle), which can be separately identified and quantified. WM connectivity can be assessed with DTI, where the streamline projections in a lateral and posterior view are shown in Fig. 13 (right top and bottom). The origin/terminus of WM streamlines can be associated with any ROI shown in the structural 3-D images, allowing a direct assessment of the pathway integrity between ROIs. What the 3-D imaging portrays, in Fig. 13, is how the

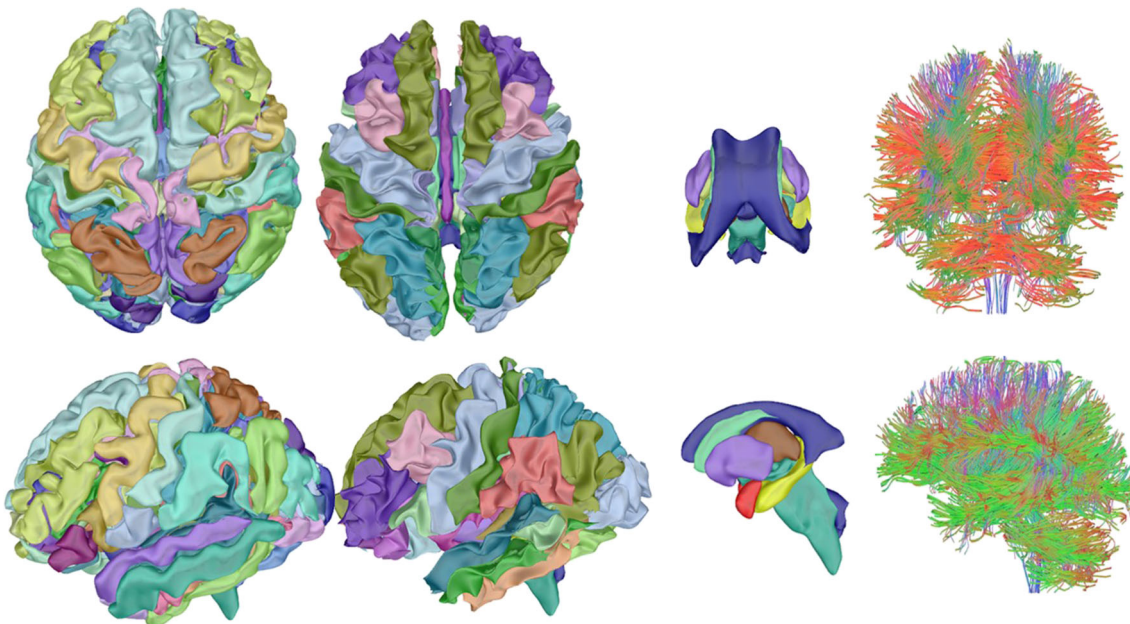


Fig. 13 Three-dimensional rendering of the cortical surface on the left. Each color reflects a difference gyrus. Middle, left depicts the cortical WM, with the GM mantle removed, to depict the cortical WM surface, also colorized according to gyral association. Middle, right depicts

subcortical structures where red = amygdala, yellow = Hippocampus, brown = thalamus, purple = putamen, blue (top) = ventricle, and aqua-marine (top) = caudate. DTI streamlines are shown on the right

individual brain can be viewed from any perspective, with shape and morphology quantified including subcortical structures (middle, top, and bottom right).

Since overall brain volume is but representative of its constituent parts, robust positive correlations between the size of a subcortical region and overall brain size is the general rule; however, dynamic subcortical growth as well as changes over time, which may also include pruning, apply to subcortical GM structures as well. For example, the plots in Fig. 14, from Foulkes and Blakemore (2018), depict different developmental changes that accompany subcortical ROIs. While some subcortical regions, as shown in Fig. 14, reflected more of a pruning decrease in volume with increasing age, reminiscent of what was observed with whole-brain GM as depicted in Fig. 4, the pallidum, thalamus, amygdala, and hippocampus did not. How these developmental differences relate to functional outcome during these developmental periods remains to be seen, but speculation would center on the complexities of social maturation that would be particularly dependent on increased regulatory roles involving thalamic integration and the social-emotional-cognitive regulation needed during the prolonged adolescent to adulthood transition. The mastery of more end-stage cognitive development and emotional control to navigate adulthood and the rest of the lifespan may be highly dependent on when cellular maturation occurs, especially subcortically. Also, the hippocampus is a region where neurogenesis occurs (Seki, 2020), which may also involve the amygdala and thalamus (Jurkowski et al., 2020). Neurogenesis and its interaction with environment may play

a role in growth trajectories of some of these structures (Dow-Edwards et al., 2019). More will be said about the hippocampus and amygdala later.

DTI, Imaging of White Matter Tracts and Their Quantification

DTI was introduced in the discussion of Figs. 12 and 13. The MR signal is based on the precession characteristics of hydrogen molecules and the physics of water diffusion. As such, the difference in tissue types of brain parenchyma is all about intracellular and extracellular water content within and between WM, GM, and CSF. With DTI technology, there is a host of what is referred to as diffusion metrics. Figure 15 provides some basic parameters of what is being measured with two DTI metrics. Assume in Fig. 15 that a drop of water strikes a surface where there are no constraints in the direction that the water disperses. For example, a water droplet on an absorbent piece of paper generates a perfect sphere of dispersion and absorption, as water goes in every direction. This is referred to as isotropic diffusion. Restricted diffusion is anisotropic. A common DTI metric to measure diffusion is referred to as fractional anisotropy (FA). The FA metric ranges from 0.0 (isotropic) to completely restricted as 1.0 (complete anisotropy), shown in Fig. 15. However, on the right-hand side of Fig. 15, the perpendicular boundaries are representative of cellular membranes, like myelin coating, that constrain the direction of water dispersion. Since neural tissue is highly

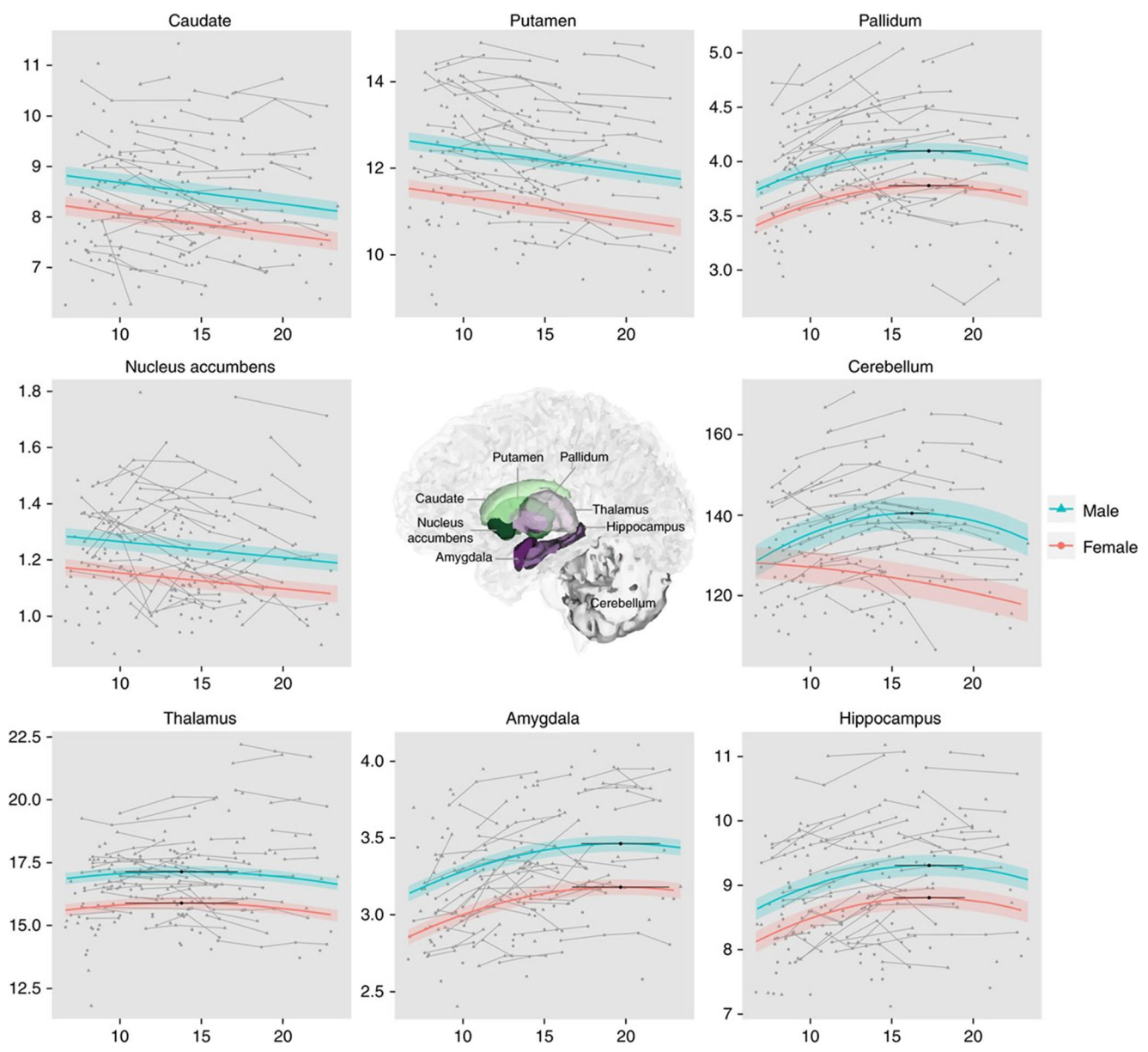


Fig. 14 Developmental trajectories for total gray matter volume: ages 7.0–23.3 years old. Mean volume in cm³ (y-axis) by age in years (x-axis) is shown for males ($n=94$, blue) and females ($n=53$, red).

Shading around the regression lines represents the 95% confidence interval of the intercept. From Foulkes and Blakemore (2018), with permission from Springer Nature

concentrated with water, being constrained by cellular membranes means that the water molecules will no longer disperse in a non-directional way, but rather in a direction perpendicular within a constraining membrane, where intracellular and extracellular water dispersion is different. In WM, the axon has two factors that constrain intracellular water: the axolemma (axon membrane) and the oligodendrocyte membrane associated with the myelin axonal coating. So, within WM, the direction of water diffusion is used to infer the orientation of axons as they aggregate together in tracts, projecting from point A to B. As indicated in Fig. 15, the colors in DTI are meaningful. Green shows the anterior-posterior orientation of WM tracts, and the blue reflects

vertically oriented tracts with the warm colors showing the left-right, side-to-side projections. If these membranes are damaged or axon integrity degrades, then water dispersion goes back to greater randomness, as shown in the lower middle image. This is also shown in the DTI color map on the left. This axial DTI image is at the level of the temporal lobe where the arrow points to a very damaged occipitotemporal fasciculus as the result of a traumatic brain injury, where the DTI color map exhibits just random water diffusion. As depicted in the cartoon, when cellular membranes have broken down, water diffuses in all directions. In contrast, look at the undamaged occipitotemporal fasciculus on the right of the image, exhibiting a distinctly bright green colorization of a normally

Diffusion Tensor Imaging

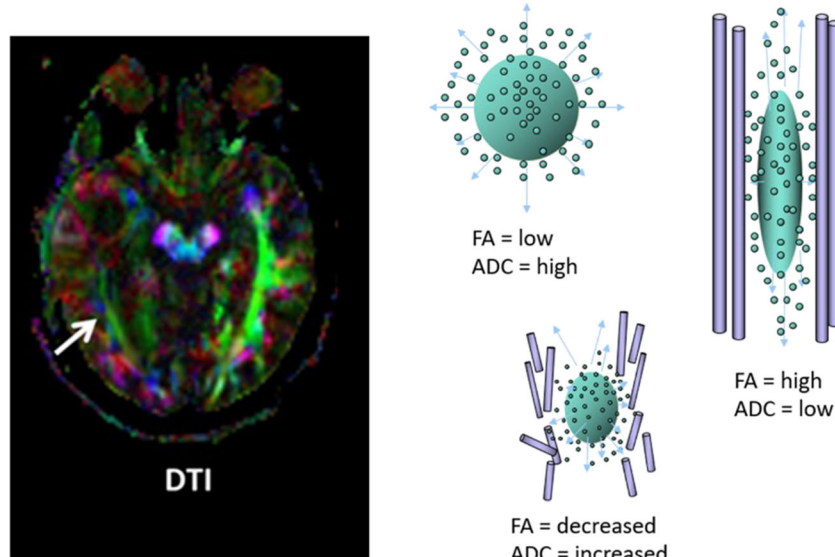


Fig. 15 Schematic depicting the principles of water diffusion, fractional anisotropy (FA), apparent diffusion coefficient (ADC), and diffusion tensor imaging (DTI). When a water droplet diffuses when unconstrained in any way, top middle image, equal water dispersion occurs in all directions. However, if water is constrained, as in the upper right image, the direction of dispersion is restricted. In DTI, the directionality of water diffusion can be used to infer directionality of WM

appearing WM tract. This indicates well-organized WM tracts all oriented in the anterior-posterior plane, which is their normal configuration at this level of the temporal lobe.

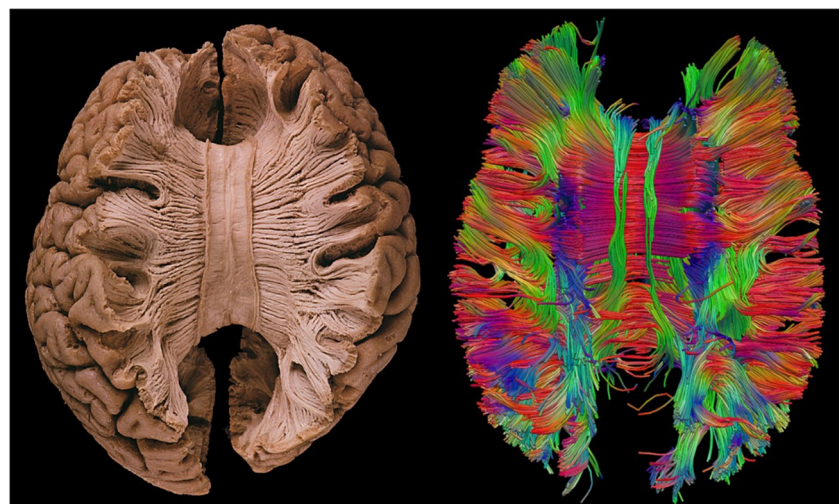
What is particularly important about DTI is that through a process referred to as tractography, aggregated WM tracks can be extracted from the scan image as depicted in Figs. 12 and 13 and in Fig. 16. The left image in Fig. 16 is a post-mortem, dorsal view of the brain where the top of the cerebral cortex has been meticulously dissected away displaying the aggregated side-to-side WM tracts projecting across midline,

tracts, as shown in the DTI color map in the lower left. Green reflects orientation in the anterior-posterior direction, blue reflects vertical orientation, and warm, orange-to-red colors reflect orientation in a lateral direction, as depicted in the lower right of the color map. However, in the presence of damage or degraded WM integrity, diffusion returns to random (lower middle schematic). For more details, see Hayes et al. (2016)

forming the corpus callosum. To the right is DTI tractography at the same level, but in a living human. Note the general agreement of the DTI image with that of the post-mortem, depicting the tracts across the corpus callosum but also including visualization of U-fibers at the cortical level. Also important is that there are numerous methods for DTI quantification of tracts as well as WM as indices of WM integrity (i.e., FA; see Oishi et al., 2013).

This technology permits not only showing all of the aggregated WM tracts in the brain, as presented in Figs. 13 and 16,

Fig. 16 (Left) Post-mortem dissection, dorsal view exposing aggregated fiber tracts coursing across the corpus callosum along with U-fibers between cortical gyri. From Gluhbegovic and Williams (1980). (Right) Dorsal DTI view of WM tract streamlines, showing how close the conform to the post-mortem anatomic image. Color scheme given in Fig. 15



but isolated as well as aggregated tracts (fasciculi) or specific ROIs can be identified and examined, as shown in Fig. 17 from Assaf et al. (2019).

This, in turn, also means that developmentally, WM tracts can be subjected to analyses at different ages, providing a more direct method for examining myelination-mediated developmental changes that reflect brain connectivity. When such methods are applied to the developing brain, familiar WM growth plots emerge from viewing DTI changes associated with development. For example, Tamnes et al. (2018) examined DTI metrics from childhood through age 32 as shown in Fig. 18.

The growth curves presented in Fig. 18 show that different trajectories exist within each tract, where FA may change or not at different stages of development. Close inspection of the individual plot lines in Fig. 18 shows interesting individual differences across regions, where there are region-specific fluctuations in FA. Tamnes et al. (2018) also show in Fig. 18 that after peak development, reductions in FA may occur. Note that some FA peaks in development or stability do not occur until after 20 years of age. The importance of

these WM changes is that they do relate to cognition and behavior as shown in the neurodevelopmental WM DTI study by Krogsrud et al. (2018) that examined DTI metrics in relation to verbal and visuospatial working memory. Figure 19 shows why these developmental changes are critically important in understanding cognitive development. Age-mediated improvements in basic working memory (top, Fig. 19) are graphically demonstrated to relate to increased FA (bottom, Fig. 19), presumed to reflect increased myelination and WM integrity, which facilitates neural connectivity and speed of processing.

Another way of viewing these changes is through plots that depict the percent change in DTI metrics, as presented in Fig. 20 (see Geeraert et al., 2019; Lebel et al., 2019; Lebel & Deoni, 2018; Mah et al., 2017). The percent change plots in Fig. 20, from Lebel et al. (2019), demonstrate that these diverse tracts respond differentially to age and development. As will be discussed in the next section, these developmental factors become meaningful in understanding the clinical and applied significance for what myelin changes mean for cognition and behavior.

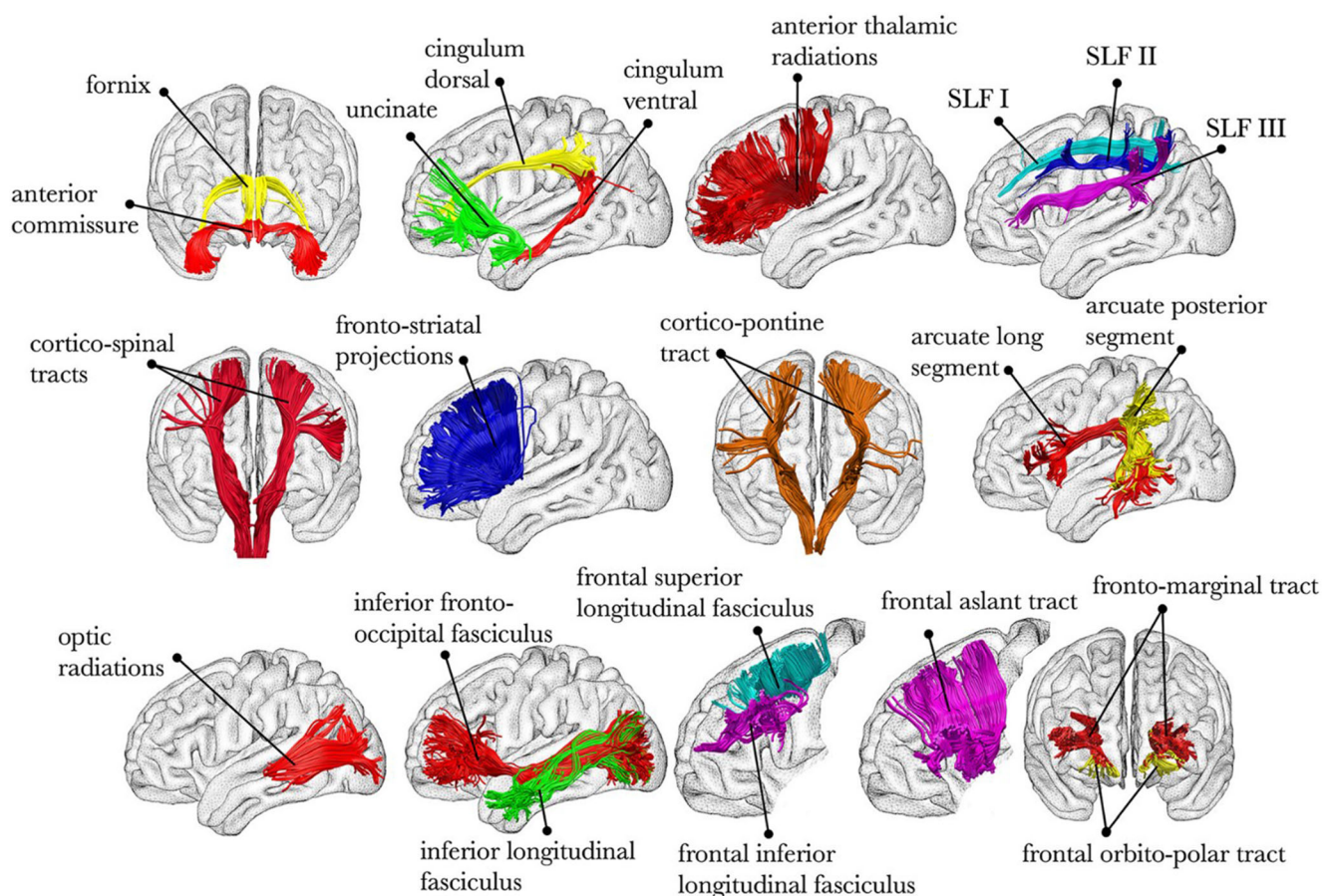


Fig. 17 Summary of some of the major DTI-derived tracts that can be extracted from a MR scan. From Assaf et al. (2019), used with permission from Wiley

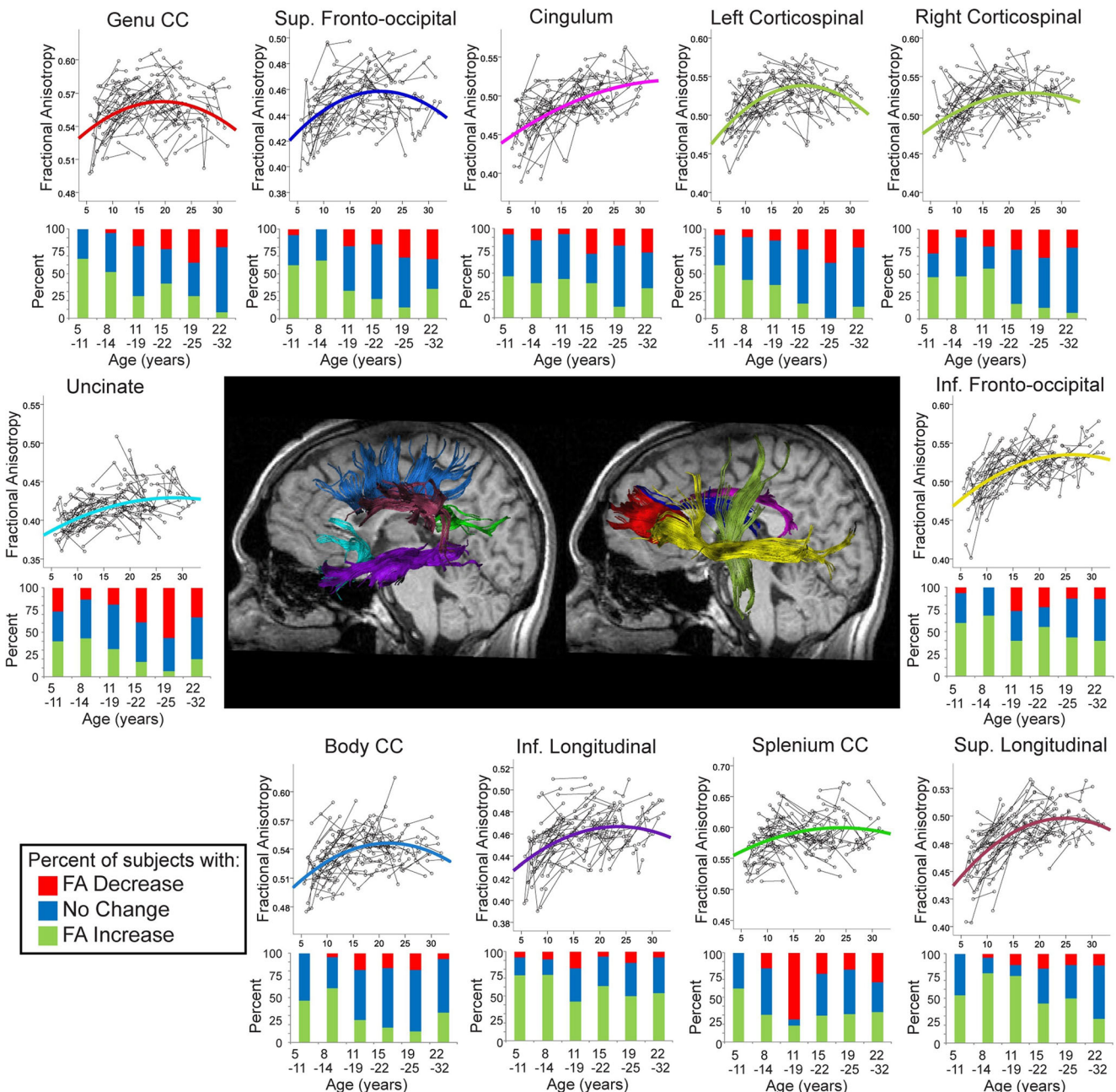


Fig. 18 Longitudinal age-related changes of fractional anisotropy (FA) in healthy individuals aged 5–32 years. Spaghetti plots with the best fitting models and bar graphs depicting the percentage of subjects whose FA increased (green), decreased (red), or did not change (blue) in six age

groupings are shown for different WM fibers, derived using a deterministic tractography method from Tamnes et al. (2018) and reproduced with permission from Elsevier

Functional Connectivity Reflective of Brain Maturity

The increases in WM volume in the healthy, age-typical individual, as inferred from the above discussion, reflect both myelination and increased functional connectivity throughout the brain (Bells et al., 2019; Haber et al.,

2020). There is a variety of functional neuroimaging-based connectivity metrics that can be applied, one of which uses the fMRI signal as described in Fig. 12. At rest, brain regions that have similar and synchronous BOLD activity are likely connected (Le et al., 2020). This is referred to as resting-state (rs), functional connectivity (fc) MRI or rs-fcMRI mapping (Dosenbach et al.,

2010). In the developing brain, as networks become established, WM connectivity is enhanced which can be inferred from the coherence of rs-fcMRI signals. Accordingly, measuring network complexity over developmental periods of time represents another approach related to brain maturation, myelination, and connectivity. Returning to Fig. 16 and the dorsal view showing the side-to-side homotopic visualization of aggregate WM tracts that project to their homologue within each cortical area, it becomes straightforward to understand that these brain regions are also connected. This, in turn, means that for regions connected when at rest, they should display similar levels of brain activation (i.e., BOLD signal), recorded in rs-fcMRI pattern activation, where increased connectivity levels likely occur in relation to age and maturation. This is reflected in the study by Dosenbach et al. (2010) and displayed in Fig. 21 (see also Becht & Mills, 2020). While the plots in Fig. 21 are similar to the structural imaging of WM growth, importantly, these fMRI-based functional connectivity indicators also specify that WM maturation is similarly expressed in physiological changes.

In the plots shown in Fig. 22, Somerville (2016) argues that by assessing when asymptote levels are achieved across various neuroimaging metrics including functional connectivity, as described above, this point of stabilization likely heralds a range wherein maturity is reached. However, as shown in the plots from Somerville (2016) as well as throughout this

review, there are major regional and individual differences that likely point to a varied maturation rate related to structural and functional brain development.

Sex Differences

In many of the studies reviewed so far, sex differences have to be statistically controlled for, so group data could be presented. Becht and Mills (2020) review methods and findings that examine individual differences in brain development, that start first with differences between males and females. Head size does relate to body size, and from the perspective of body size, on average, males have larger bodies than females. This also means they have larger absolute head/brain size. As such, this gets reflected in different volumes which are demonstrated in Fig. 23. In this illustration, the plot represents the reduction in cortical gray matter volume of the prefrontal cortex with similar trajectory slopes regardless of sex, although the absolute values are less in females. Figure 14 shows that these sex difference-mediated effects occur throughout all subcortical areas.

In the largest lifespan study to examine sex differences to date, Wierenga et al. (2020), as part of the Enhancing Neuro-Imaging Genetics through Meta-Analysis (ENIGMA) international effort to combine neuroimaging datasets, studied 16,683 healthy individuals 1–90 years old, where 47% were female. The following was observed: “... greater male than

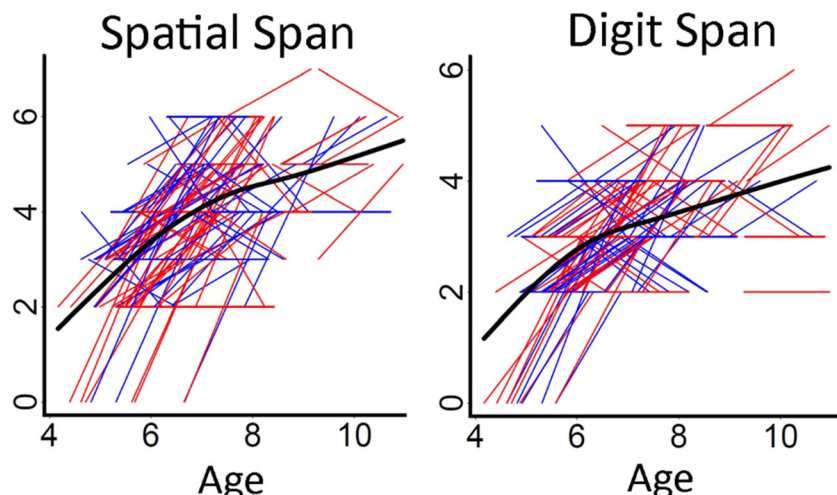


Fig. 19 (Top) Spatial Span Backward and Digit Span Backward scores with age. Spaghetti plots of individual participant change in Spatial Span Backward and Digit Span Backward scores with age (years). Females are plotted in red and males in blue. For each measure, an assumption-free general additive mixed model as a function of age was fitted to accurately describe group-level changes across the age range. From Krogsrud et al. (2018), used with permission (<https://doi.org/10.1371/journal.pone.0195540.g001>). (Bottom) FA change in visuospatial working memory. Scatterplots showing linear relationships between change in FA and change in visuospatial working memory. The plots show FA in the

inferior fronto-occipital fasciculus (IFOF, yellow) and forceps major (FMaj, red), plotted as z-transform change values. For Spatial Span Backward scores, age, sex, and interval are regressed out, and for each tract ROI, age, sex, interval, and motion at both time points are regressed out. The partial correlation (r) between change in FA in specific white matter tracts and change in Spatial Span Backward scores, controlling for age, sex, interval, and motion at both time points, is presented in each plot. From Krogsrud et al. (2018), used with permission (<https://doi.org/10.1371/journal.pone.0195540.g002>)

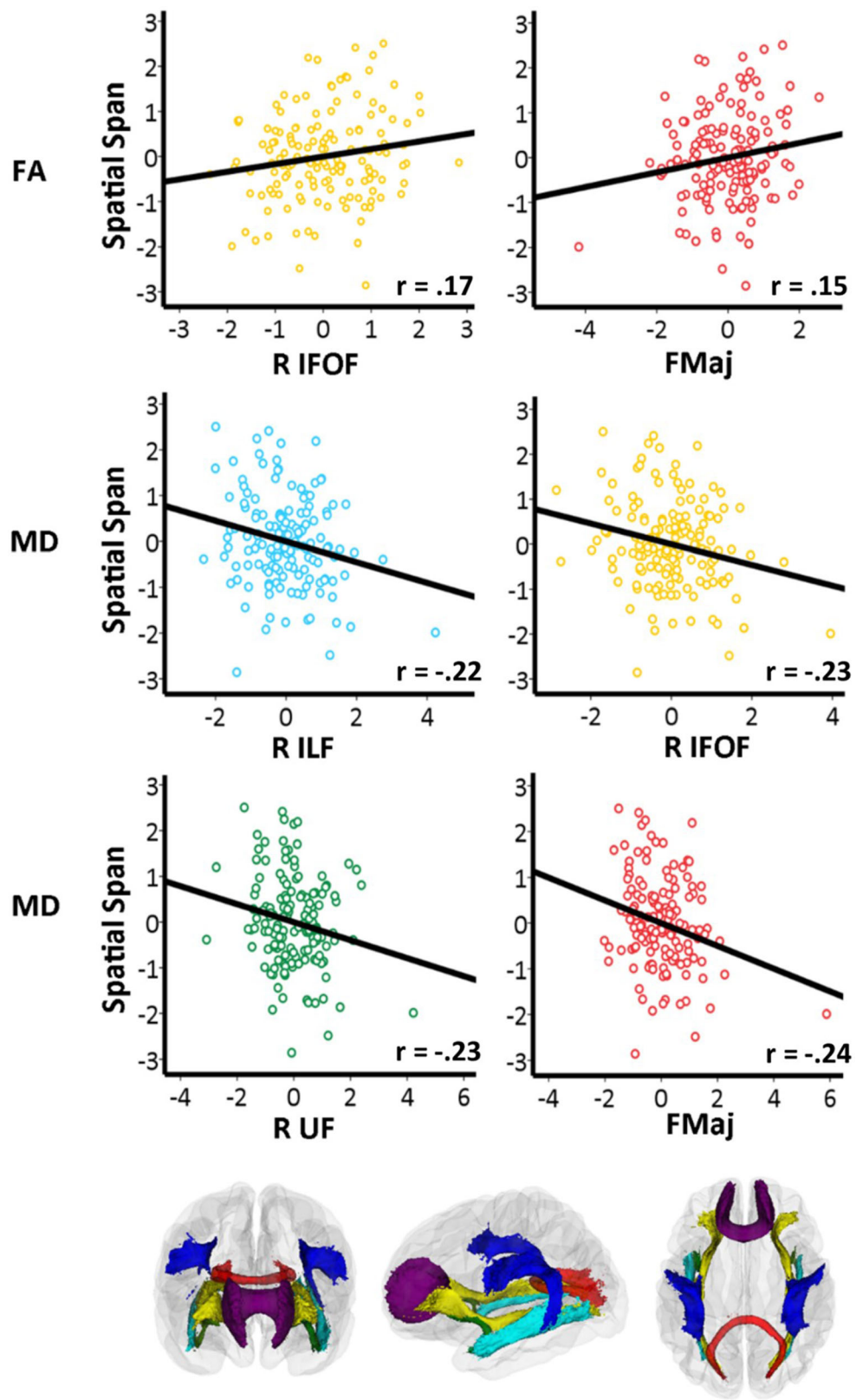


Fig. 19 (continued)

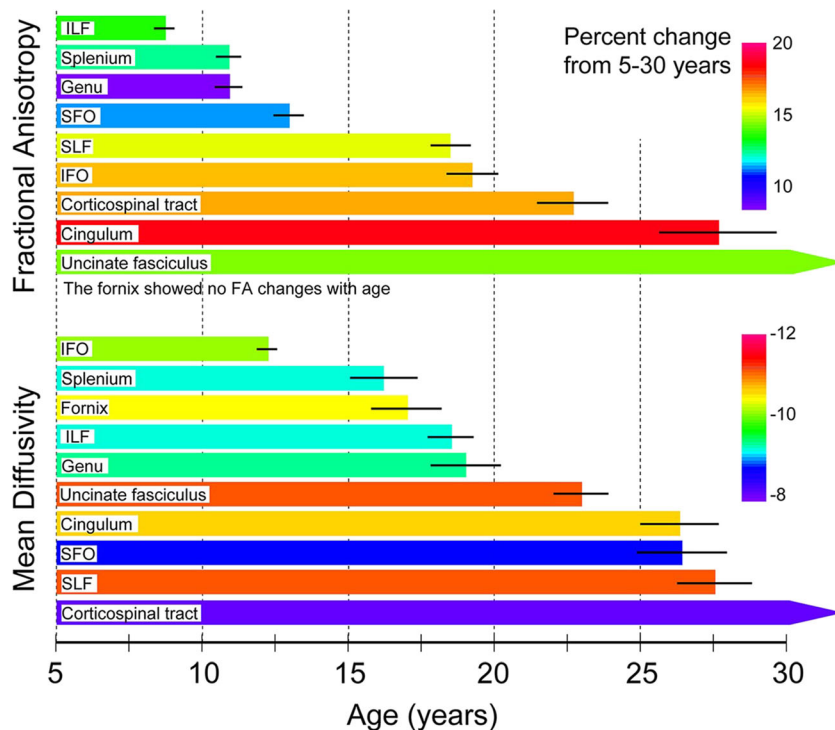


Fig. 20 A Yakovlev-inspired 2 plot showing FA and mean diffusivity (MD) timing profiles of 10 major white matter tracts. MD is a measure that reflects total diffusion within a voxel. The end of the horizontal bar reflects the age at which either FA or MD reaches 90% of its exponential plateau value from 5 to 30 years of age, as outlined by Lebel et al. (2008).²⁷ Some tracts level off in the pre-teen years and others in the late teens, and a few tracts continue developing into the 20s (e.g., the corticospinal

tract, frontal-temporal cingulum, and uncinate fasciculus). The callosal tracts tend to mature earlier, although the order of maturation differs depending on whether one is measuring MD or FA. Note also that, in general, peak maturation of MD is reached at older ages than FA for the same white matter tract. Hot colors reflect greater proportional FA or MD changes from 5 years to the plateau. From Lebel et al. (2019), reproduced with permission from Wiley Publishing

female between-subject variance for all subcortical volumetric measures, all cortical surface area measures, and 60% of cortical thickness measures.” This pattern was stable across the lifespan for 50% of the subcortical structures, 70% of the regional area measures, and nearly all regions for thickness (p., currently e-pub). These investigators conclude that “The findings highlight the importance of individual differences within the sexes, that may underpin sex-specific vulnerability to disorders.” Accordingly, all future neuroimaging studies involving brain development need to more substantially address sex differences.

Networks

All of these advanced neuroimaging analyses reviewed above only become relevant to the field of neuropsychology when viewed in the context of how they relate to function. Up to this point, a specific structure or ROI has been plotted over a developmental trajectory showing change over time. However, every structure or ROI is only important in its relation to one another and its participation in neural networks. Accordingly, function, and what a pediatric neuropsychologist may assess as part of a

neuropsychological examination, is all about connectivity and how a specific brain structure or ROI connects with other parts of the brain that results in cognition and behavior. Using a fMRI approach, Yeo et al. (2014) and Yeo et al. (2011) derived cortical maps of some of the major functional networks based on a ROI and cortical parcellation method and how these regions connect during task-specific activities using some of the fMRI techniques described above. This is presented in Fig. 21.

As shown in Fig. 24, while an oversimplification, as there are far more networks than the seven presented, for demonstrable purposes, this does show that all networks involve multiple brain regions along with the connectivity between the two hemispheres. While what is shown in Fig. 24 is MRI based, similar network topologies come from activation patterns derived from electrophysiological procedures as well as other functional neuroimaging methods like positron emission tomography, often integrated with MRI methods for network analysis (Prajapati & Emerson, 2020). Accordingly, the networks shown in Fig. 24 have been consistently demonstrated and are considered reasonable approximations of established neural networks for the domains color coded in the illustration. Importantly, what is shown in Fig. 24 is only the cortical representation and activation story, representing

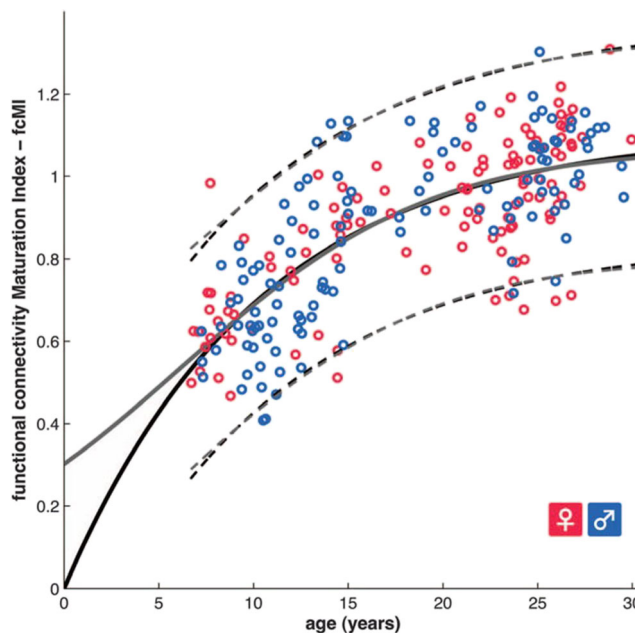


Fig. 21 Functional brain maturation curve. Individual functional brain maturity levels of 238 rs-fcMRI scans (115 females) between the ages of 7 and 30 years. Chronological age is shown on the x-axis and the fcMRI on the y-axis (females: pink, males: blue). The fit for the von Bertalanffy equation ($a(1 - e^{-bx})$, $r^2 = 0.553$, permutation test, $P < 0.001$, AIC weight = 0.3) is shown with a solid black line. The fit for the Pearl-Reed equation ($a / (1 + b \cdot e^{-cx})$, $r^2 = 0.555$, AIC weight = 0.23) is shown with a solid gray line. The 95% prediction limits are shown with dashed lines. From Dosenbach et al. (2010), used with permission from the American Association for the Advancement of Science

only a part of the network. Not shown are all of the subcortical-to-cortical connectivity networks. Accordingly, when thinking about brain networks, no sensory experience, with the partial exception of olfaction, does not register in cortical activation without initial subcortical activation. What

has been covered so far has shown how individual ROIs can be identified and quantified in terms of their volume, size, shape, thickness, and/or some other physical metrics and how WM connectivity can be assessed with DTI and fMRI techniques. All of these factors have to come together to best understand network integrity and function and its relationship with neuropsychological outcome in the developing brain. Ultimately, it is not about a solitary ROI, but the integration across the network. Because many of the methods described in this review have just been refined within the last decade, the application of these neuroimaging findings to network image analysis and brain development is just in the earliest stages (Dow-Edwards et al., 2019; Kast & Levitt, 2019; Thomason, 2020).

As part of the twenty-first-century connectome project (see <https://nrg.wustl.edu/nrg-projects/hcp/>), a variety of elegant methods has evolved using advanced neuroimaging methods to establish and study brain networks. For example, Sotiropoulos and Zalesky (2019) provide an excellent review for how this can be achieved that would have relevance for understanding brain maturation and neuropsychological outcome. From a network perspective, each network probably has its own unique maturation sequence. For example, in Fig. 24, the visual and somatomotor networks based on neurobehavioral data likely reach asymptote earlier than the more cognitive networks, with the limbic-emotional network probably the last (Braun, 2011). As neuroimaging methods improve in the quantification of network neuroscience, it is anticipated that more specific timeframes associated with network maturation will also be forthcoming. As shown in Fig. 9, it is likely that the ability for neuropsychological measures to better assess brain-behavior relations would be improved, if different neurobehavioral and neurocognitive measures could be directly linked to neuroimaging-derived brain age coefficients.

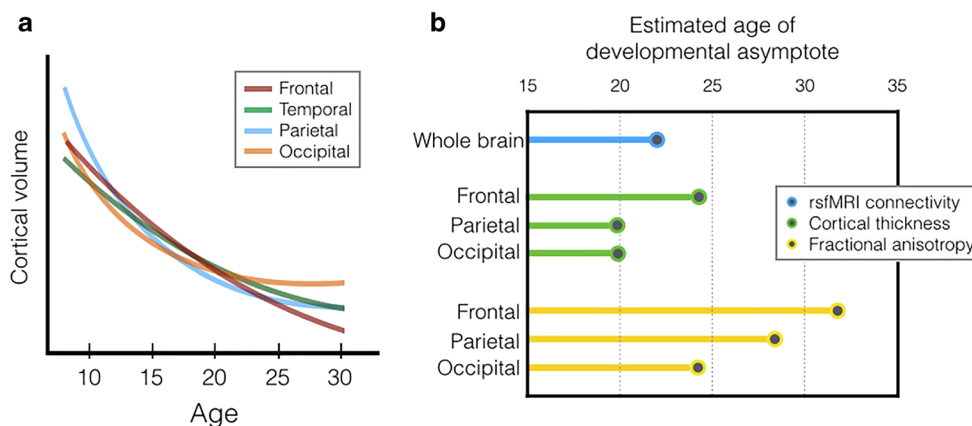
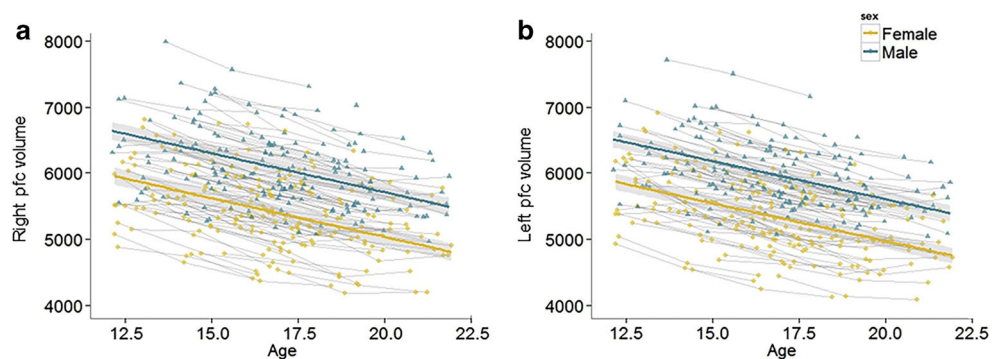


Fig. 22 Regional and Methodological Variance in Neurodevelopmental Indices from Somerville (2016). **a** Trajectories of cortical gray matter volume adjusting for total brain volume. Trajectories are schematized from data reported in Ostby et al. (2009). **b** Ages of developmental

asymptote for connectivity and structural data. Resting-state, functional connectivity MRI (rs-fcMRI) data from Dosenbach et al. (2010) and the other measures reflect data reported in Tamnes et al. (2010). Note that the operationalization of “asymptote” varies by study

Fig. 23 Observed individual volume (in mm³) trajectories and average trajectories for **a** right prefrontal cortical volume and **b** left prefrontal cortical volume. Shaded areas represent 95% confidence interval. Raw mean scores for prefrontal cortical volume are displayed. pfc = prefrontal cortex. From Becht and Mills (2020), used with permission from Elsevier



Clinical Significance of Neuroimaging-Derived Indices of Brain Development

Brain Development and Neuropsychiatric Disorder: Adverse Childhood Experiences

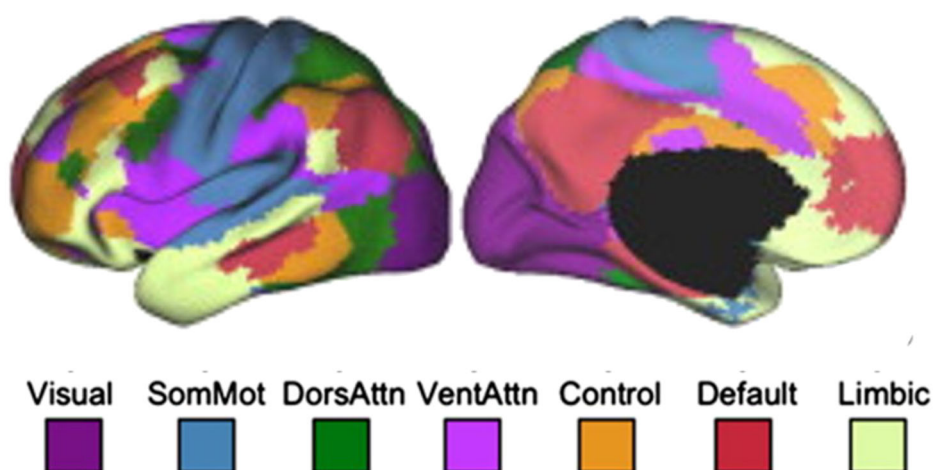
Normal neural development is experience dependent (Holtmaat & Svoboda, 2009). This, in turn, means that experience shapes neural circuits and connectivity. From what has been reviewed above, this also means that certain environments, external factors, and influences may impact both structural development (i.e., size) and neural communication (i.e., connectivity).

Considerable research has now been conducted on children, adolescents, and adults who have experienced childhood maltreatment. How does that maltreatment affect brain development and does the stage of brain development at the point where an adverse childhood experience (ACE) occurs influence brain development onward (Braun & Bock, 2011)? Table 1, from Danese and McEwen (2012), while a decade

old, still represents a summary of some of the neuroimaging and physiological measures associated with adverse childhood experiences (see also Anda et al., 2006; Herzog & Schmalh, 2018).

Since all aspects of brain development are sensitive to experience-dependent influences throughout maturation, it is no surprise that issues related to ACE factor into brain development. As described in this review, the methods for image analysis are relatively new, so the emerging literature on the potential effects of ACE as revealed in quantitative neuroimaging is also just in its initial stage. Socioeconomic status (SES) has long been examined in the context of child development, not only because of SES relations to health and nutrition but also because of educational opportunities and parenting (Steele et al., 2016). Figure 25 is from McDermott et al. (2019) that examined a larger cohort of 623 youth who underwent structural MRI with volumetric and shape analyses. They observed a strong positive association between SES and TBV as well as with both total WM and GM volumes. Cortical surface area was also positively correlated, and while cortical thickness was as well, it exhibited the least robust

Fig. 24 Neuroimaging-derived, 7-network schemata. From Yeo et al. (2014), used with permission from Elsevier Publishing



Visual: Visual network; SomMot: somatomotor network; DorsAttn: dorsal attention network; VentAttn: ventral attention network; Control: frontoparietal control network; Default: default network; Limbic: limbic network.

Table 1 Summary of the brain, endocrine, and immune correlates of childhood maltreatment in children and adult individuals

	Children	Adults
Brain	Prefrontal cortex: smaller volume, poorer executive functions Amygdala: possibly larger volume Hippocampus: no changes Behavior: poorer attention, greater activity levels, impaired emotion regulation, and self-regulatory behaviors	Prefrontal cortex: smaller volume Amygdala: possibly smaller volume, greater startle response Hippocampus: smaller volume, deficit in declarative memory Behavior: depression, PTSD, substance abuse
HPA axis	Basal levels: higher cortisol levels, flatter cortisol profile TSST: blunted cortisol response	Basal levels: higher CRH levels TSST: blunted (no mental illness) or heightened (with mental illness) control response
Immune system	Pharmacological stimulation: blunted ACTH response and normal cortisol response to CRH test (heightened ACTH response in depressed + maltreated) Innate immunity: elevated inflammation levels (in depressed + maltreated) Acquired immunity: poorer response to latent HSV infection	Pharmacological stimulation: blunted (no mental illness) or heightened (with mental illness) ACTH and cortisol responses to DEX/CRH test Innate immunity: elevated inflammation levels Acquired immunity: high T cytotoxic cell/T helper cell ratio, greater type IV hypersensitivity response

relationship. As shown in Fig. 25, greater SES was also significantly associated with all subcortical ROIs examined except the pallidum.

While Fig. 25 shows the influence of SES on hippocampal and amygdala volume controlling for age, when examining their trajectories over age and by sex, as

shown in Fig. 26 from Fish et al. (2020), there are important points of trajectory inflection and peak development. Note that for both structures, changes extend into the 20s. Integrating the investigation of McDermott et al. (2019) with that of Fish et al. (2020), which both focused on the hippocampus and

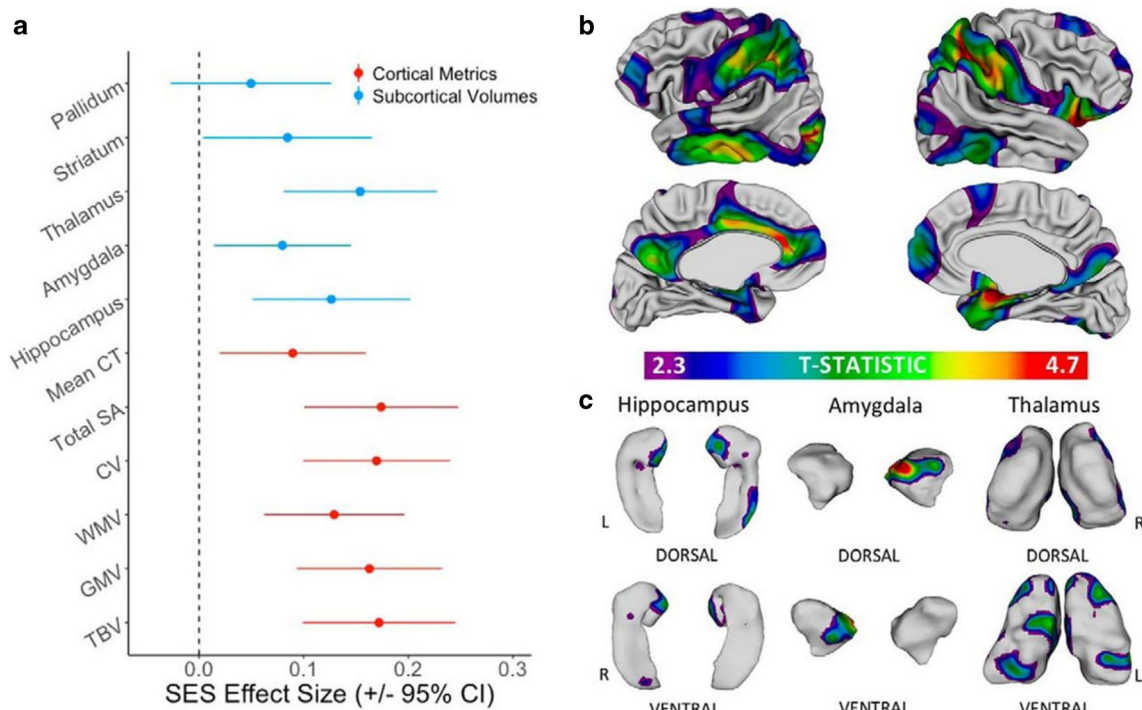


Fig. 25 Main effects of SES on global and local anatomy after controlling for age and sex. **a** Standardized effect size of SES on each global cortical and subcortical brain measure estimated using scaled variables: TBV, GMV, WMV, CV, SA, mean CT, hippocampus volume, amygdala volume, thalamus volume, striatum volume, and pallidum volume. **b**

Cortical surface regions that show a significant positive association of surface area with childhood SES. **c** Subcortical surface regions that show a significant positive association of surface area with childhood SES

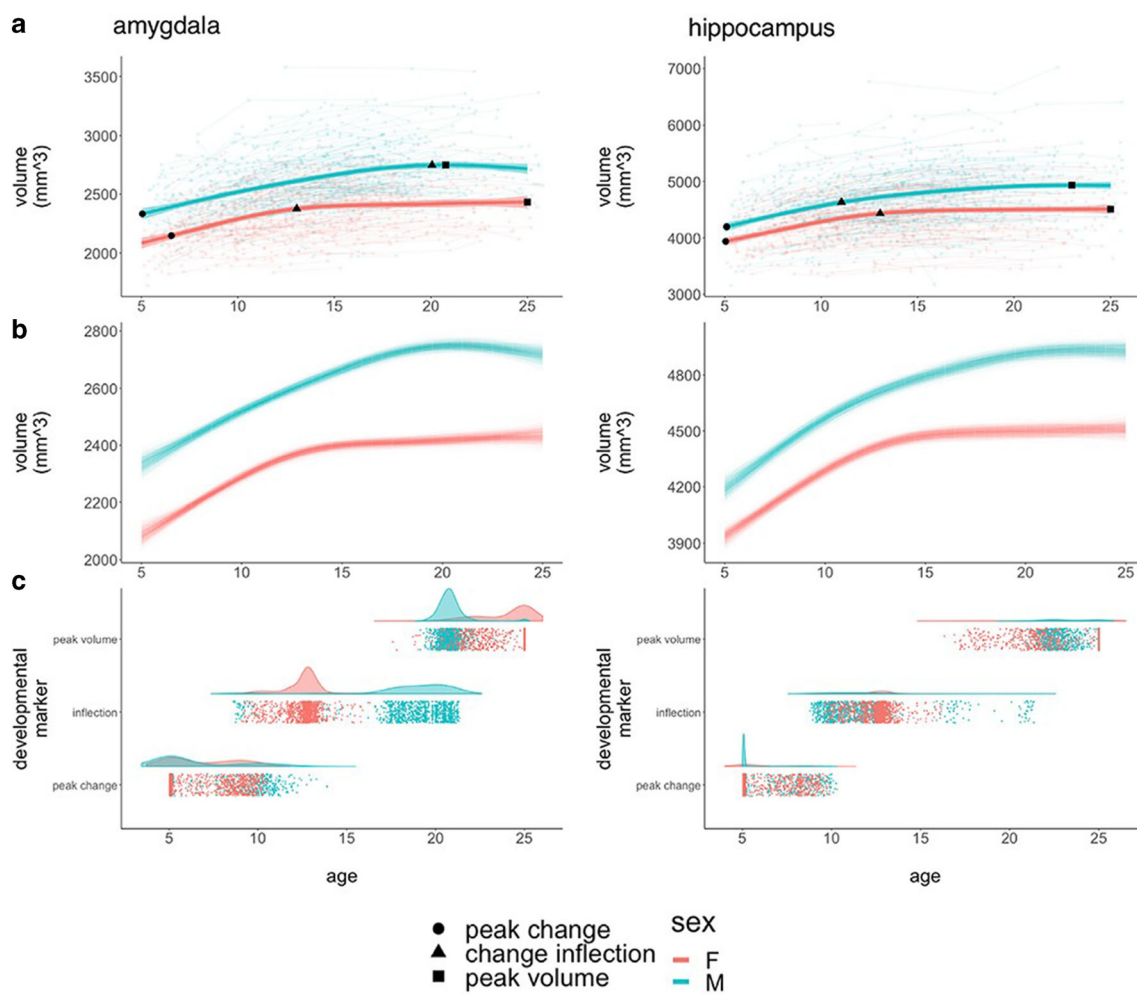


Fig. 26 Developmental curves and milestones for bulk amygdalar and hippocampal volume. **a** Spline-based, group-level trajectories for the bulk bilateral volume of each structure are shown by sex (males = blue/females = red). These fit lines are superimposed on spaghetti plots of raw data showing individual volume measurements (background circles), linked by lines denoting observations from the same individual. Fit lines are surrounded by shaded 95% confidence intervals. The three developmental markers (i.e., age of fastest volume change [circles], age of greatest change in developmental tempo [triangles], and age at attainment of peak

volume [squares]) overlay the fit lines for each sex and for each structure. **b** Spline-based, group-level trajectories for the bulk bilateral volume of each structure from 1000 bootstrap samples of our data, where we resampled from the set of 792 individuals with replacement. **c** Visualization of developmental milestone timing distributions across bootstrap samples, stratified by sex, where each point corresponds to the timing of a developmental milestone in a bootstrap sample. From Fish et al. (2020), with permission from Elsevier

amygdala from a developmental perspective, these two structures that are so important to cognitive control and emotional regulation have a two-decade timeframe of potential vulnerability from ACE effects.

In their review of ACE effects on the brain, Teicher et al. (2016) review the literature and speculate on additional ROIs as well as neural networks that may be most affected by abuse, maltreatment, and neglect. These are diagrammatically presented in Fig. 27. Because of the intimate relations between experience, the environment, and rapid brain growth with changes in the developing brain, the degree, type, and actual changes in brain structure and function that result from ACE influence await longitudinal research.

Brain Development and Acquired Injury

The timing of when a brain injury occurs within the developmental trajectory of an ROI influences how that region develops from the point of injury on. The degree of gyration as shown in Fig. 10 relates to brain development, but it can also be an index associated with what happens when the brain is injured. For example, Wilde et al. (2020) found an altered pattern of expected development in cortical gyration in children who had sustained a traumatic injury to the brain, with changes in late-developing frontal and parietal areas particularly altered. In addition to whatever focal pathology that may occur from acquired brain injury, developmentally, how such changes in brain

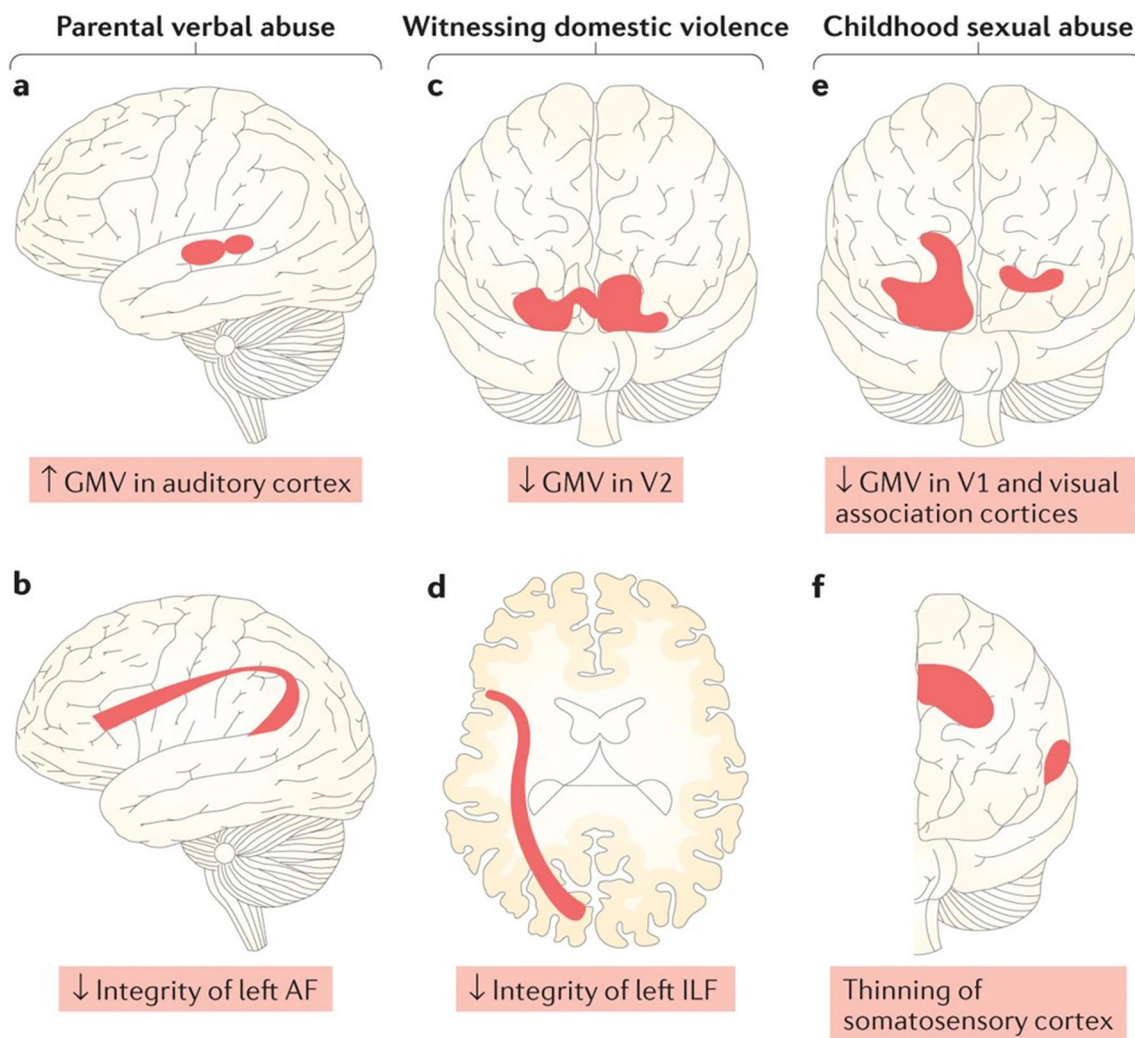


Fig. 27 Images depicting the potential effects of exposure to specific types of childhood maltreatment on gray matter volume (GMV) or thickness and fiber tract integrity. Exposure to parental verbal abuse was associated with increased GMV in the auditory cortex portion of the left superior temporal gyrus 25 (part a) and decreased integrity of the left arcuate fasciculus (AF) interconnecting Wernicke's area and Broca's area 26 (part b). Visually witnessing multiple episodes of domestic violence was associated with reduced GMV in the right lingual gyrus, left occipital pole, and bilateral secondary visual cortex (V2) 27 (part c) and with

Nature Reviews | Neuroscience

decreased integrity of the left inferior longitudinal fasciculus (ILF), which serves as a visual-limbic pathway (part d). Adults reporting exposure to multiple episodes of childhood forced-contact sexual abuse were found to have reduced GMV in the right and left primary visual cortex (V1) and visual association cortices, as well as reduced thickness in right lingual, left fusiform, and left middle occipital gyri (part e) and portions of the somatosensory cortex representing the genital area (part f). See Teicher et al. (2016) for additional research details that form the basis for these images. Reproduced with permission from Springer Nature Publishing

structure alter patterns of neural maturation and network development contributes to the chronicity of cognitive and behavioral deficits. Alternatively, Wilde et al. (2020) also observed increased gyration in some brain-injured children, which, over time, may reflect "... a compensatory mechanism that allows for typical development of cortical surface area, despite reduced brain volume." Ewing-Cobbs et al. (2016) and Wilde et al. (2012a) have shown that the

age of injury influences WM integrity of corpus callosum development. There is a paucity of research in this area as to how the timing of acquired brain pathology affects outcome, brain development after injury, and the contributions that neuroimaging could provide (Greenham et al., 2020). This also means a lack of studies relating pediatric neuropsychological findings in relation to acquired injury and neuroimaging.

Summary

As this review is being published, there are major, multi-site investigations of brain development as part of the Adolescent Brain Cognitive Development (ABCD, see Karcher & Barch, 2021) investigation and the previously mentioned ENIGMA project (see Dennis et al., 2020). There are others as well that will be multi-site and possess sample sizes and diverse participant backgrounds to address the statistical power necessary to further and more accurately address the complex issues raised in this review. From all of the images and growth plots presented in this review, the brain goes through dynamic changes in the first three decades of life that can be quantified with neuroimaging. Also, to date, pediatric neuropsychology has not taken advantage of these unprecedented methods in image quantification to better utilize a brain-age metric (Franke & Gaser, 2019; Jiang et al., 2019), integrated with neuropsychological assessment. One of the other aspects of quantitative neuroimaging is that the analysis methods are becoming more and more automated (Oishi et al., 2013), which, to date, has been advanced primarily in adult neuroimaging (Goodkin et al., 2019; Pemberton et al., 2021). Nonetheless, with large normative and publicly accessible neuroimaging datasets and rapid automated output, it is anticipated that this information will become available for all aspects of research and clinical application in pediatric neuropsychology.

Acknowledgements Dr. Bigler is retired with emeritus and adjunct status at the institutions listed above. Dr. Bigler provides forensic consultation.

References

- Ambrose, J., & Hounsfield, G. (1973). Computerized transverse axial tomography. *The British Journal of Radiology*, 46(542), 148–149. Retrieved from <https://www.ncbi.nlm.nih.gov/pubmed/4686818>.
- Anaturk, M., Kaufmann, T., Cole, J. H., Suri, S., Griffanti, L., Zsoldos, E., et al. (2020). Prediction of brain age and cognitive age: Quantifying brain and cognitive maintenance in aging. *Human Brain Mapping*. <https://doi.org/10.1002/hbm.25316>.
- Anda, R. F., Felitti, V. J., Bremner, J. D., Walker, J. D., Whitfield, C., Perry, B. D., et al. (2006). The enduring effects of abuse and related adverse experiences in childhood. A convergence of evidence from neurobiology and epidemiology. *European Archives of Psychiatry and Clinical Neuroscience*, 256(3), 174–186. <https://doi.org/10.1007/s00406-005-0624-4>.
- Assaf, Y., Johansen-Berg, H., & Thiebaut de Schotten, M. (2019). The role of diffusion MRI in neuroscience. *NMR in Biomedicine*, 32(4), e3762. <https://doi.org/10.1002/nbm.3762>.
- Ball Jr., W. S. (1991). Imaging of the brain in children. *Current Opinion in Radiology*, 3(6), 895–905. Retrieved from <https://www.ncbi.nlm.nih.gov/pubmed/1751299>.
- Baron, I. S. (2018). *Neuropsychological evaluation of the child*. Oxford University Press.
- Becht, A. I., & Mills, K. L. (2020). Modeling individual differences in brain development. *Biological Psychiatry*, 88(1), 63–69. <https://doi.org/10.1016/j.biopsych.2020.01.027>.
- Bells, S., Lefebvre, J., Longoni, G., Narayanan, S., Arnold, D. L., Yeh, E. A., & Mabbott, D. J. (2019). White matter plasticity and maturation in human cognition. *Glia*, 67(11), 2020–2037. <https://doi.org/10.1002/glia.23661>.
- Bigler, E. D. (2017). Structural neuroimaging in neuropsychology: History and contemporary applications. *Neuropsychology*, 31(8), 934–953. <https://doi.org/10.1037/neu0000418>.
- Bigler, E. D., Abildskov, T. J., Goodrich-Hunsaker, N. J., Black, G., Christensen, Z. P., Huff, T., et al. (2016). Structural neuroimaging findings in mild traumatic brain injury. *Sports Medicine and Arthroscopy Review*, 24(3), e42–e52. <https://doi.org/10.1097/JSA.0000000000000119>.
- Blinkov, S. M., & Glezer, I. I. (1968). *The human brain in figures and tables: A quantitative handbook*. Basic Books.
- Braun, K. (2011). The prefrontal-limbic system: Development, neuroanatomy, function, and implications for socioemotional development. *Clinics in Perinatology*, 38(4), 685–702. <https://doi.org/10.1016/j.clp.2011.08.013>.
- Braun, K., & Bock, J. (2011). The experience-dependent maturation of prefronto-limbic circuits and the origin of developmental psychopathology: Implications for the pathogenesis and therapy of behavioural disorders. *Developmental Medicine and Child Neurology*, 53(Suppl 4), 14–18. <https://doi.org/10.1111/j.1469-8749.2011.04056.x>.
- Coma, M., Valls, R., Mas, J. M., Pujol, A., Herranz, M. A., Alonso, V., & Naval, J. (2014). Methods for diagnosing perceived age on the basis of an ensemble of phenotypic features. *Clinical, Cosmetic and Investigational Dermatology*, 7, 133–137. <https://doi.org/10.2147/CCID.S52257>.
- Courchesne, E., Chisum, H. J., Townsend, J., Cowles, A., Covington, J., Egas, B., et al. (2000). Normal brain development and aging: Quantitative analysis at in vivo MR imaging in healthy volunteers. *Radiology*, 216(3), 672–682. <https://doi.org/10.1148/radiology.216.3.r00au37672>.
- Danese, A., & McEwen, B. S. (2012). Adverse childhood experiences, allostasis, allostatic load, and age-related disease. *Physiology & Behavior*, 106(1), 29–39. <https://doi.org/10.1016/j.physbeh.2011.08.019>.
- Davison, A. N., & Dobbing, J. (1966). Myelination as a vulnerable period in brain development. *British Medical Bulletin*, 22(1), 40–44. <https://doi.org/10.1093/oxfordjournals.bmb.a070434>.
- Dennis, E. L., Baron, D., Bartnik-Olson, B., Caeyenberghs, K., Esopenko, C., Hillary, F. G., et al. (2020). ENIGMA brain injury: Framework, challenges, and opportunities. *Human Brain Mapping*. <https://doi.org/10.1002/hbm.25046>.
- Dosenbach, N. U., Nardos, B., Cohen, A. L., Fair, D. A., Power, J. D., Church, J. A., et al. (2010). Prediction of individual brain maturity using fMRI. *Science*, 329(5997), 1358–1361. <https://doi.org/10.1126/science.1194144>.
- Dow-Edwards, D., MacMaster, F. P., Peterson, B. S., Niesink, R., Andersen, S., & Braams, B. R. (2019). Experience during adolescence shapes brain development: From synapses and networks to normal and pathological behavior. *Neurotoxicology and Teratology*, 76, 106834. <https://doi.org/10.1016/j.ntt.2019.106834>.
- Ernhart, C. B. (1991). Clinical correlations between ethanol intake and fetal alcohol syndrome. *Recent Developments in Alcoholism*, 9, 127–150. Retrieved from <https://www.ncbi.nlm.nih.gov/pubmed/1758980>.
- Eskenazi, B., Gaylord, L., Bracken, M. B., & Brown, D. (1988). In utero exposure to organic solvents and human neurodevelopment. *Developmental Medicine and Child Neurology*, 30(4), 492–501. <https://doi.org/10.1111/j.1469-8749.1988.tb04776.x>.
- Ewing-Cobbs, L., Johnson, C. P., Juranek, J., DeMaster, D., Prasad, M., Duque, G., et al. (2016). Longitudinal diffusion tensor imaging after pediatric traumatic brain injury: Impact of age at injury and time

- This document is copyrighted by the American Psychological Association or one of its allied publishers. This article is intended solely for the personal use of the individual user and is not to be disseminated broadly.
- since injury on pathway integrity. *Human Brain Mapping*, 37(11), 3929–3945. <https://doi.org/10.1002/hbm.23286>.
- Fish, A. M., Nadig, A., Seidlitz, J., Reardon, P. K., Mankiw, C., McDermott, C. L., et al. (2020). Sex-biased trajectories of amygdalo-hippocampal morphology change over human development. *Neuroimage*, 204, 116122. <https://doi.org/10.1016/j.neuroimage.2019.116122>.
- Foulkes, L., & Blakemore, S. J. (2018). Studying individual differences in human adolescent brain development. *Nature Neuroscience*, 21(3), 315–323. <https://doi.org/10.1038/s41593-018-0078-4>.
- Franke, K., & Gaser, C. (2019). Ten years of BrainAGE as a neuroimaging biomarker of brain aging: What insights have we gained? *Frontiers in Neurology*, 10, 789. <https://doi.org/10.3389/fneur.2019.00789>.
- Freiwald, W. A. (2020). The neural mechanisms of face processing: Cells, areas, networks, and models. *Current Opinion in Neurobiology*, 60, 184–191. <https://doi.org/10.1016/j.conb.2019.12.007>.
- Fu, Y., Guo, G., & Huang, T. S. (2010). Age synthesis and estimation via faces: A survey. *IEEE Transactions on Pattern Analysis and Machine Intelligence*, 32(11), 1955–1976. <https://doi.org/10.1109/TPAMI.2010.36>.
- Geeraert, B. L., Lebel, R. M., & Lebel, C. (2019). A multiparametric analysis of white matter maturation during late childhood and adolescence. *Human Brain Mapping*, 40(15), 4345–4356. <https://doi.org/10.1002/hbm.24706>.
- Gilmore, J. H., Knickmeyer, R. C., & Gao, W. (2018). Imaging structural and functional brain development in early childhood. *Nature Reviews Neuroscience*, 19(3), 123–137. <https://doi.org/10.1038/nrn.2018.1>.
- Gluhbegovic, N., & Williams, T. H. (1980). *The human brain: A photographic guide*. Harper & Row.
- Goodkin, O., Pemberton, H., Vos, S. B., Prados, F., Sudre, C. H., Moggridge, J., et al. (2019). The quantitative neuroradiology initiative framework: Application to dementia. *The British Journal of Radiology*, 92(1101), 20190365. <https://doi.org/10.1259/bjr.20190365>.
- Greenham, M., Botchway, E., Knight, S., Bonyhady, B., Tavender, E., Scheinberg, A., et al. (2020). Predictors of participation and quality of life following major traumatic injuries in childhood: A systematic review. *Disability and Rehabilitation*, 1–17. <https://doi.org/10.1080/09638288.2020.1849425>.
- Haber, S. N., Tang, W., Choi, E. Y., Yendiki, A., Liu, H., Jbabdi, S., et al. (2020). Circuits, networks, and neuropsychiatric disease: Transitioning from anatomy to imaging. *Biological Psychiatry*, 87(4), 318–327. <https://doi.org/10.1016/j.biopsych.2019.10.024>.
- Hayes, J. P., Bigler, E. D., & Verfaellie, M. (2016). Traumatic brain injury as a disorder of brain connectivity. *Journal of the International Neuropsychological Society*, 22(2), 120–137. <https://doi.org/10.1017/S1355617715000740>.
- Herculano-Houzel, S. (2009). The human brain in numbers: A linearly scaled-up primate brain. *Frontiers in Human Neuroscience*, 3, 31. <https://doi.org/10.3389/neuro.09.031.2009>.
- Herschkowitz, N., & Rossi, E. (1971). Critical periods in brain development. In: Lipids, malnutrition & the developing brain. *Ciba Found Symp*, 107–119. <https://doi.org/10.1002/9780470719862.ch7>.
- Herzog, J. I., & Schmahl, C. (2018). Adverse childhood experiences and the consequences on neurobiological, psychosocial, and somatic conditions across the lifespan. *Frontiers in Psychiatry*, 9, 420. <https://doi.org/10.3389/fpsyg.2018.00420>.
- Holtmaat, A., & Svoboda, K. (2009). Experience-dependent structural synaptic plasticity in the mammalian brain. *Nature Reviews Neuroscience*, 10(9), 647–658. <https://doi.org/10.1038/nrn2699>.
- Insel, T. R., & Landis, S. C. (2013). Twenty-five years of progress: The view from NIMH and NINDS. *Neuron*, 80(3), 561–567. <https://doi.org/10.1016/j.neuron.2013.09.041>.
- Jiang, H., Lu, N., Chen, K., Yao, L., Li, K., Zhang, J., & Guo, X. (2019). Predicting brain age of healthy adults based on structural MRI parcellation using convolutional neural networks. *Frontiers in Neurology*, 10, 1346. <https://doi.org/10.3389/fneur.2019.01346>.
- Jurkowski, M. P., Bettio, L., Woo, E. K., Patten, A., Yau, S. Y., & Gil-Mohapel, J. (2020). Beyond the hippocampus and the SVZ: Adult neurogenesis throughout the brain. *Frontiers in Cellular Neuroscience*, 14, 576444. <https://doi.org/10.3389/fncel.2020.576444>.
- Karcher, N. R., & Barch, D. M. (2021). The ABCD study: Understanding the development of risk for mental and physical health outcomes. *Neuropsychopharmacology*, 46(1), 131–142. <https://doi.org/10.1038/s41386-020-0736-6>.
- Kast, R. J., & Levitt, P. (2019). Precision in the development of neocortical architecture: From progenitors to cortical networks. *Progress in Neurobiology*, 175, 77–95. <https://doi.org/10.1016/j.pneurobio.2019.01.003>.
- Krogsrud, S. K., Fjell, A. M., Tamnes, C. K., Grydeland, H., Due-Tonnessen, P., Bjørnerud, A., et al. (2018). Development of white matter microstructure in relation to verbal and visuospatial working memory-A longitudinal study. *PLoS One*, 13(4), e0195540. <https://doi.org/10.1371/journal.pone.0195540>.
- Le, T. M., Huang, A. S., O’Rawe, J., & Leung, H. C. (2020). Functional neural network configuration in late childhood varies by age and cognitive state. *Developmental Cognitive Neuroscience*, 45, 100862. <https://doi.org/10.1016/j.dcn.2020.100862>.
- Lebel, C., & Deoni, S. (2018). The development of brain white matter microstructure. *Neuroimage*, 182, 207–218. <https://doi.org/10.1016/j.neuroimage.2017.12.097>.
- Lebel, C., Walker, L., Leemans, A., Phillips, L., Beaulieu, C. (2008). Microstructural maturation of the human brain from childhood to adulthood 40(3):1044–1055. <https://doi.org/10.1016/j.neuroimage.2007.12.053>.
- Lebel, C., Treit, S., & Beaulieu, C. (2019). A review of diffusion MRI of typical white matter development from early childhood to young adulthood. *NMR in Biomedicine*, 32(4), e3778. <https://doi.org/10.1002/nbm.3778>.
- Lindsey, H. M., Wilde, E. A., Caeyenberghs, K., & Dennis, E. L. (2019). Longitudinal neuroimaging in pediatric traumatic brain injury: Current state and consideration of factors that influence recovery. *Frontiers in Neurology*, 10, 1296. <https://doi.org/10.3389/fneur.2019.01296>.
- Mah, A., Geeraert, B., & Lebel, C. (2017). Detailing neuroanatomical development in late childhood and early adolescence using NODDI. *PLoS One*, 12(8), e0182340. <https://doi.org/10.1371/journal.pone.0182340>.
- Maxeiner, H., & Behnke, M. (2008). Intracranial volume, brain volume, reserve volume and morphological signs of increased intracranial pressure—A post-mortem analysis. *Legal Medicine (Tokyo, Japan)*, 10(6), 293–300. <https://doi.org/10.1016/j/legalmed.2008.04.001>.
- McDermott, C. L., Seidlitz, J., Nadig, A., Liu, S., Clasen, L. S., Blumenthal, J. D., et al. (2019). Longitudinally mapping childhood socioeconomic status associations with cortical and subcortical morphology. *The Journal of Neuroscience*, 39(8), 1365–1373. <https://doi.org/10.1523/JNEUROSCI.1808-18.2018>.

- This document is copyrighted by the American Psychological Association or one of its allied publishers. This article is intended solely for the personal use of the individual user and is not to be disseminated broadly.
- Meredith, H. V. (1946). Physical growth from birth to two years; head circumference; a review and synthesis of North American research on groups of infants. *Child Development*, 17(1-2), 1–61. Retrieved from <https://www.ncbi.nlm.nih.gov/pmc/articles/PMC21002136/>.
- Murphy, C. A. (2011). *The role of perception in age estimation*. Springer.
- Novikov, D. S., Fieremans, E., Jespersen, S. N., & Kiselev, V. G. (2019). Quantifying brain microstructure with diffusion MRI: Theory and parameter estimation. *NMR in Biomedicine*, 32(4), e3998. <https://doi.org/10.1002/nbm.3998>.
- Oishi, K., Faria, A. V., Yoshida, S., Chang, L., & Mori, S. (2013). Quantitative evaluation of brain development using anatomical MRI and diffusion tensor imaging. *International Journal of Developmental Neuroscience*, 31(7), 512–524. <https://doi.org/10.1016/j.ijdevneu.2013.06.004>.
- Ostby Y, Tammes CK, Fjell AM, Westlye LT, Due-Tønnessen P, Walhovd KB (2009) Heterogeneity in subcortical brain development: A structural magnetic resonance imaging study of brain maturation from 8 to 30 years. *J Neurosci* 29(38):11772–11782. <https://doi.org/10.1523/JNEUROSCI.1242-09.2009>
- Pemberton, H. G., Goodkin, O., Prados, F., Das, R. K., Vos, S. B., Moggridge, J., et al. (2021). Automated quantitative MRI volumetry reports support diagnostic interpretation in dementia: A multi-rater, clinical accuracy study. *European Radiology*. <https://doi.org/10.1007/s00330-020-07455-8>.
- Pfefferbaum, A., Mathalon, D. H., Sullivan, E. V., Rawles, J. M., Zipursky, R. B., & Lim, K. O. (1994). A quantitative magnetic resonance imaging study of changes in brain morphology from infancy to late adulthood. *Archives of Neurology*, 51(9), 874–887. <https://doi.org/10.1001/archneur.1994.00540210046012>.
- Pinto, P. S., Meoded, A., Poretti, A., Tekes, A., & Huisman, T. A. (2012). The unique features of traumatic brain injury in children. Review of the characteristics of the pediatric skull and brain, mechanisms of trauma, patterns of injury, complications, and their imaging findings—Part 2. *Journal of Neuroimaging*, 22(2), e18–e41. <https://doi.org/10.1111/j.1552-6569.2011.00690.x>.
- Prajapati, R., & Emerson, I. A. (2020). Construction and analysis of brain networks from different neuroimaging techniques. *The International Journal of Neuroscience*, 1–22. <https://doi.org/10.1080/00207454.2020.1837802>.
- Pujol, J., Soriano-Mas, C., Ortiz, H., Sebastian-Galles, N., Losilla, J. M., & Deus, J. (2006). Myelination of language-related areas in the developing brain. *Neurology*, 66(3), 339–343. <https://doi.org/10.1212/01.wnl.0000201049.66073.8d>.
- Raznahan, A., Shaw, P., Lalonde, F., Stockman, M., Wallace, G. L., Greenstein, D., et al. (2011). How does your cortex grow? *The Journal of Neuroscience*, 31(19), 7174–7177. <https://doi.org/10.1523/JNEUROSCI.0054-11.2011>.
- Reynolds, C. R., & Fletcher-Janzen, E. (2009). *Handbook of clinical child neuropsychology* (3rd ed.). Springer.
- Ryan, N. P., Anderson, V. A., Bigler, E. D., Dennis, M., Taylor, H. G., Rubin, K. H., et al. (2020). Delineating the nature and correlates of social dysfunction after childhood traumatic brain injury using common data elements: Evidence from an international multi-cohort study. *Journal of Neurotrauma*. <https://doi.org/10.1089/neu.2020.7057>.
- Schmitt, J. E., Raznahan, A., Clasen, L. S., Wallace, G. L., Pritikin, J. N., Lee, N. R., et al. (2019). The dynamic associations between cortical thickness and general intelligence are genetically mediated. *Cerebral Cortex*, 29(11), 4743–4752. <https://doi.org/10.1093/cercor/bhz007>.
- Schurz, M., Radua, J., Tholen, M. G., Maliske, L., Margulies, D. S., Mars, R. B., et al. (2020). Toward a hierarchical model of social cognition: A neuroimaging meta-analysis and integrative review of empathy and theory of mind. *Psychological Bulletin*. <https://doi.org/10.1037/bul0000030>.
- Seki, T. (2020). Understanding the real state of human adult hippocampal neurogenesis from studies of rodents and non-human primates. *Frontiers in Neuroscience*, 14, 839. <https://doi.org/10.3389/fnins.2020.00839>.
- Serru, M., Marechal, B., Kober, T., Ribier, L., Sembely Taveau, C., Sirinelli, D., et al. (2019). Improving diagnosis accuracy of brain volume abnormalities during childhood with an automated MP2RAGE-based MRI brain segmentation. *Journal of Neuroradiology*. <https://doi.org/10.1016/j.neurad.2019.06.005>.
- Silk, T. J., Genc, S., Anderson, V., Efron, D., Hazell, P., Nicholson, J. M., et al. (2016). Developmental brain trajectories in children with ADHD and controls: A longitudinal neuroimaging study. *BMC Psychiatry*, 16, 59. <https://doi.org/10.1186/s12888-016-0770-4>.
- Somerville, L. H. (2016). Searching for signatures of brain maturity: What are we searching for? *Neuron*, 92(6), 1164–1167. <https://doi.org/10.1016/j.neuron.2016.10.059>.
- Sotiropoulos, S. N., & Zalesky, A. (2019). Building connectomes using diffusion MRI: Why, how and but. *NMR in Biomedicine*, 32(4), e3752. <https://doi.org/10.1002/nbm.3752>.
- Steele, H., Bate, J., Steele, M., Dube, S. R., Danskin, K., Knafo, H., et al. (2016). Adverse childhood experiences, poverty, and parenting stress. *Canadian Journal of Behavioural Science / Revue canadienne des sciences du comportement*, 48(1), 32–38. <https://doi.org/10.1037/cbs0000034>.
- Tammes CK, Ostby Y, Fjell AM, Westlye LT, Due-Tønnessen P, Walhovd KB (2010) Brain maturation in adolescence and young adulthood: regional age-related changes in cortical thickness and white matter volume and microstructure. *Cereb Cortex* 20(3):534–548. <https://doi.org/10.1093/cercor/bhp118>
- Tammes, C. K., Roalf, D. R., Goddings, A. L., & Lebel, C. (2018). Diffusion MRI of white matter microstructure development in childhood and adolescence: Methods, challenges and progress. *Developmental Cognitive Neuroscience*, 33, 161–175. <https://doi.org/10.1016/j.dcn.2017.12.002>.
- Teicher, M. H., Samson, J. A., Anderson, C. M., & Ohashi, K. (2016). The effects of childhood maltreatment on brain structure, function and connectivity. *Nature Reviews Neuroscience*, 17(10), 652–666. <https://doi.org/10.1038/nrn.2016.111>.
- Thomason, M. E. (2020). Development of brain networks in utero: Relevance for common neural disorders. *Biological Psychiatry*, 88(1), 40–50. <https://doi.org/10.1016/j.biopsych.2020.02.007>.
- van Osch, M. J., Teeuwisse, W. M., Chen, Z., Suzuki, Y., Helle, M., & Schmid, S. (2018). Advances in arterial spin labelling MRI methods for measuring perfusion and collateral flow. *Journal of Cerebral Blood Flow and Metabolism*, 38(9), 1461–1480. <https://doi.org/10.1177/0271678X17713434>.
- Veraart, J., Nunes, D., Rudrapatna, U., Fieremans, E., Jones, D. K., Novikov, D. S., & Shemesh, N. (2020). Noninvasive quantification of axon radii using diffusion MRI. *eLife*, 9. <https://doi.org/10.7554/eLife.49855>.
- Vidal-Pineiro, D., Parker, N., Shin, J., French, L., Grydeland, H., Jackowski, A. P., et al. (2020). Cellular correlates of cortical thinning throughout the lifespan. *Scientific Reports*, 10(1), 21803. <https://doi.org/10.1038/s41598-020-78471-3>.
- Walhovd, K. B., Fjell, A. M., Giedd, J., Dale, A. M., & Brown, T. T. (2017). Through thick and thin: A need to reconcile contradictory results on trajectories in human cortical development. *Cerebral Cortex*, 27(2), 1472–1481. <https://doi.org/10.1093/cercor/bhv301>.

- Wierenga, L. M., Doucet, G. E., Dima, D., Agartz, I., Aghajani, M., Akudjedu, T. N., et al. (2020). Greater male than female variability in regional brain structure across the lifespan. *Human Brain Mapping*. <https://doi.org/10.1002/hbm.25204>.
- Wilde, E. A., McCauley, S. R., Barnes, A., Wu, T. C., Chu, Z., Hunter, J. V., & Bigler, E. D. (2012a). Serial measurement of memory and diffusion tensor imaging changes within the first week following uncomplicated mild traumatic brain injury. *Brain Imaging and Behavior*, 6(2), 319–328. <https://doi.org/10.1007/s11682-012-9174-3>.
- Wilde, E. A., Hunter, J. V., & Bigler, E.D. (2012b). A primer of neuro-imaging analysis in neurorehabilitation outcome research. *NeuroRehabilitation*, 31(3), 227–242. <https://doi.org/10.3233/NRE-2012-0793>.
- Wilde, E. A., Merkley, T. L., Lindsey, H. M., Bigler, E. D., Hunter, J. V., Ewing-Cobbs, L., et al. (2020). Developmental alterations in cortical organization and socialization in adolescents who sustained a traumatic brain injury in early childhood. *Journal of Neurotrauma*. <https://doi.org/10.1089/neu.2019.6698>.
- Willerman, L., Schultz, R., Rutledge, J. N., & Bigler, E. D. (1991). In vivo brain size and intelligence. *Intelligence*, 15(2), 223–228. [https://doi.org/10.1016/0160-2896\(91\)90031-8](https://doi.org/10.1016/0160-2896(91)90031-8).
- Yamada, S., Esaki, Y., & Mizutani, T. (1999). Intracranial cavity volume can be accurately estimated from the weights of intracranial contents: Confirmation by the dental plaster casting method. *Neuropathology and Applied Neurobiology*, 25(4), 341–344. <https://doi.org/10.1046/j.1365-2990.1999.00183.x>.
- Yeo, B. T., Krienen, F. M., Sepulcre, J., Sabuncu, M. R., Lashkari, D., Hollinshead, M., et al. (2011). The organization of the human cerebral cortex estimated by intrinsic functional connectivity. *Journal of Neurophysiology*, 106(3), 1125–1165. <https://doi.org/10.1152/jn.00338.2011>.
- Yeo, B. T., Krienen, F. M., Chee, M. W., & Buckner, R. L. (2014). Estimates of segregation and overlap of functional connectivity networks in the human cerebral cortex. *Neuroimage*, 88, 212–227. <https://doi.org/10.1016/j.neuroimage.2013.10.046>.

Publisher's Note Springer Nature remains neutral with regard to jurisdictional claims in published maps and institutional affiliations.